Marine and Petroleum Geology 100 (2019) 148–164

Contents lists available at ScienceDirect

Marine and Petroleum Geology

journal homepage: www.elsevier.com/locate/marpetgeo

Research paper

Effects of progressive burial on matrix porosity and permeability of dolostones in the foreland basin of the Alpine Orogen, Switzerland

Lukas Aschwanden*, Larryn W. Diamond, Arthur Adams

Rock–Water Interaction, Institute of Geological Sciences, University of Bern, Baltzerstrasse 3, CH-3012, Bern, Switzerland

ARTICLE INFO

Keywords:
Dolomite
Porosity
Permeability
Compaction
Burial
Molasse basin

ABSTRACT

The changes in rock-matrix porosity and permeability that carbonate reservoirs undergo with increasing burial depth are poorly understood. This lack of understanding raises the risks involved in exploring and engineering deep reservoirs for geo-energy applications. To provide more insight into compaction processes, the present study examines the effects of progressive burial on two dolomitized mudstone units belonging to the Middle Triassic Muschelkalk within the Swiss Molasse Basin, situated in the foreland of the Alpine Orogen. Based on investigations of wireline logs and drill cores retrieved from up to 5000 m depth, we report the burial modification of crystal textures, pore sizes, pore geometries and their impact on matrix porosity and permeability. Within the first 1500 m below surface, porosity is found to drop from 40 ± 2 to 18 ± 1 vol% and permeability drops from 105 ± 15 to ~1 mD. At depths > 3000 m, porosity and permeability maintain nearly constant values of 6 ± 2 vol% and < 0.01 mD, respectively. These trends are due to the cumulative effects of a series of partly concurrent processes: at depths < 1200–1900 m, mechanical rotation and fracturing of the euhedral dolomite crystals promotes closer packing and constitutes the dominant porosity-reducing mechanism; at depths > 1900 m, mechanical compaction is inactive and pressure solution at crystal contacts and along stylolites (both diagenetic and tectonic), without any associated cementation, accounts for porosity loss. At depths > 3000 m, collapse of pores by pressure solution is compounded by pore-clogging by hydrothermal dolomite introduced by external fluids. Throughout the entire depth range, stylolitization incrementally thins the formations, however, the dissolved material is not locally reprecipitated.

1. Introduction

Carbonate reservoirs are not only of interest as hydrocarbon sources (Ehrenberg and Nadeau, 2005) but also as potential storage reservoirs for injected gases (seasonal methane and anthropogenic CO_2; Chadwick et al., 2007) and as sources of geothermal heat (Goldscheider et al., 2010). Dolostones are of particular interest because they tend to have higher porosity and permeability at great depth than associated limestones (Ehrenberg et al., 2006 and references therein) and hence they offer greater potential as deep reservoirs (Purser et al., 1994; Sun, 1995). Their different behaviour relative to limestones is mainly due to their higher physical strength (Hugman and Friedman, 1979) and chemical stability (Bathurst, 1971), which render them more resistant to burial compaction (Schmoker and Halley, 1982; Saller and Henderson, 1998).

Despite the long-standing research interest in carbonate rocks, their burial compaction trends, i.e. porosity versus depth and permeability versus depth, are not well understood (Choquette and Steinen, 1980; Ehrenberg, 2006). Prediction of their reservoir properties at depth is notably difficult because it depends on so many factors: primary properties inherited from the broad spectrum of depositional environments (Bathurst, 1971); the high chemical reactivity of carbonate minerals (Moore, 2001); the complex interaction between chemical and mechanical compaction mechanisms; and the wide variety of other diagenetic modifications that occur during progressive burial (Croizé et al., 2013). Predictability of porosity and permeability losses at depth is nonetheless a key to successful exploration. Exploration companies have therefore addressed this problem intensively but relatively few studies of carbonate compaction have been published in the open literature (Croizé et al., 2013).

The present study contributes to this topic by examining the compaction effects of progressive burial on two Middle Triassic dolostone units within the Swiss Molasse Basin (Fig. 1), situated in the foreland of the waning Alpine continental-collision zone. The two dolostone units are known by their German names as the Trigonodus Dolomit (belonging to the Upper Muschelkalk stratigraphic unit) and the Dolomit

* Corresponding author.
E-mail address: lukas.aschwanden@geo.unibe.ch (L. Aschwanden).

https://doi.org/10.1016/j.marpetgeo.2018.10.055
Received 20 August 2018; Received in revised form 22 October 2018; Accepted 31 October 2018
Available online 03 November 2018

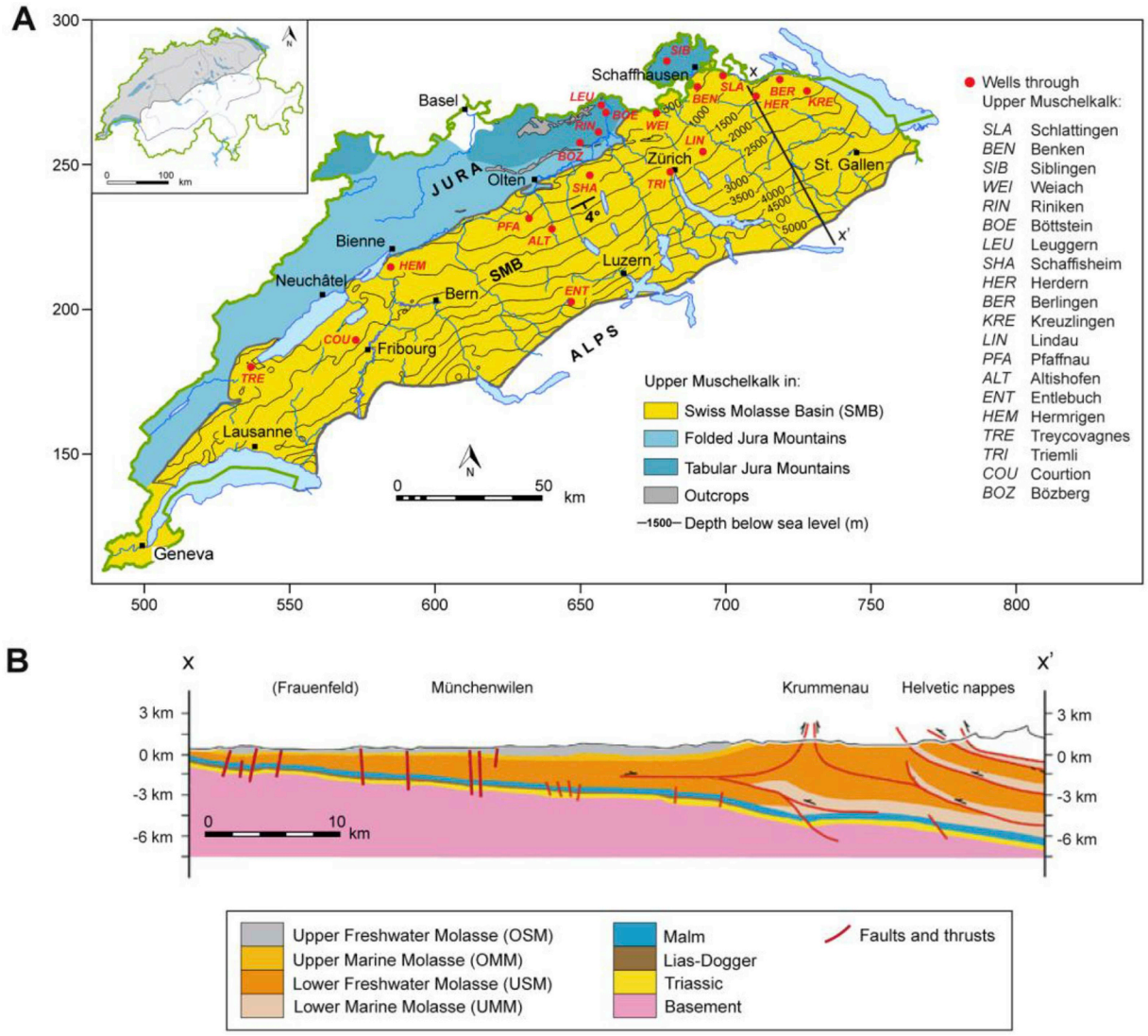

Fig. 1. Tectonic and stratigraphic settings of the Triassic Upper Muschelkalk dolostones in the Swiss Molasse Basin (SMB). (A) Tectonic map showing the extent and depth (m b.s.l.) of the Upper Muschelkalk in the Foreland of the Swiss Alps. Red dots mark wells penetrating the Upper Muschelkalk. Thick green line is the Swiss national border. Coordinates are Swiss km grid (modified after Chevalier et al., 2010; Jordan, 2016 and Sommaruga et al., 2012). (B) Stratigraphic cross-section x–x' (modified after Pfiffner et al., 1997). The Upper Muschelkalk lies within the yellow "Triassic" layer. (For interpretation of the references to colour in this figure legend, the reader is referred to the Web version of this article.)

der Anhydritgruppe (belonging to the Middle Muschelkalk stratigraphic unit) and they are currently being investigated for their potential for geothermal energy and for storage of injected gas (Chevalier et al., 2010). Herein we quantify their loss of matrix porosity and permeability with increasing burial to 5 km depth, using drill core and geophysical wireline logs. A variety of petrographic examinations of drill cores allow the observed changes in bulk rock properties to be linked to changes in microscopic features, such as crystal textures, pore sizes and pore geometries. These data then permit recognition of the contributions of mechanical and chemical compaction, as well as cementation to the overall process of progressive burial compaction.

Mechanical compaction can change the bulk rock properties of carbonate rocks by crystal fracturing, reorganization of particles or plastic deformation. In contrast, chemical compaction modifies the rock properties mainly by pressure solution (i.e. intercrystalline pressure solution or stylolitization) and it is considered to be the main porosity-reducing mechanism in carbonate rocks (e.g. Croizé et al., 2013 and references therein). Cementation, on the other hand, modifies the rock properties by precipitation of diagenetic pore-clogging minerals. The conceptual understanding gained from investigating these parameters and their impact on the bulk rock properties of carbonates during burial can be used to support predictions of the reservoir properties of deep dolostones in similar basin settings elsewhere.

2. Geological setting

The Triassic Muschelkalk belongs to the autochthonous Mesozoic sediments that cover the European crystalline basement of the Swiss Molasse Basin. The basin stretches over ~300 km along the arcuate NW margin of the Swiss Alps, widening progressively from ~30 km near Geneva in the SW to ~70 km at Constance in the NE (Fig. 1A). The basin developed during the Eocene–Miocene as the European plate flexed downwards under the emerging Alpine collisional orogen (Kempf and Pfiffner, 2004). The resulting wedge-shaped foredeep was filled by erosional debris from the Alps, such that today the Muschelkalk dips 3–5° SSE from a depth of < 1 km on the northern outer margin of the basin to > 6 km depth along the Alpine Front (Fig. 1B). The basin is still under NNW–SSE-directed compression, inherited from the orogenic convergence.

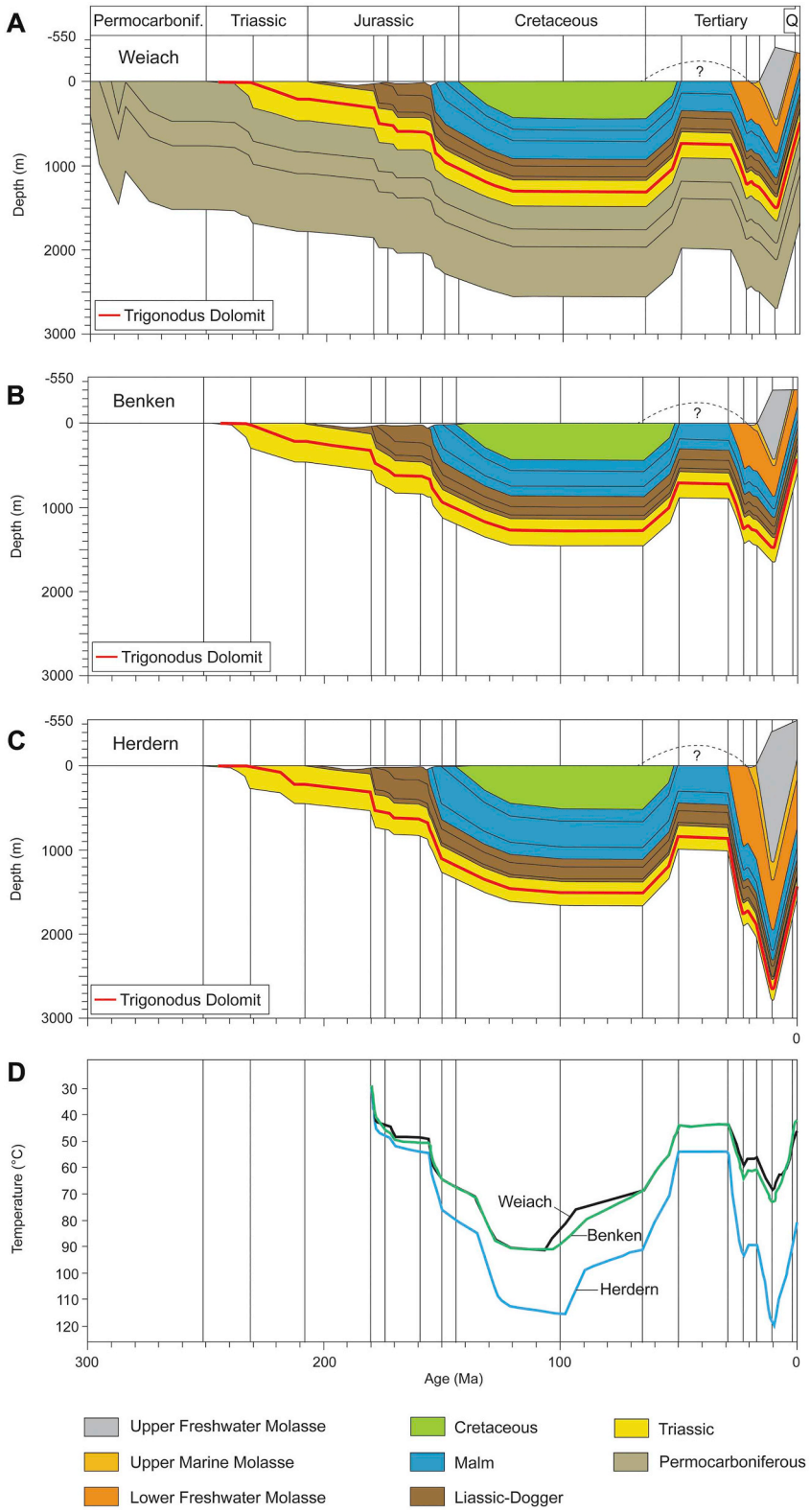

Fig. 2. Burial history of the Mesozoic–Cenozoic sediments in the NE Swiss Molasse Basin, reconstructed at selected wells (modified after Nagra, 2002). Red line in A, B, C marks Upper Muschelkalk. (A) Weiach well. (B) Benken well. (C) Herden well. (D) Reconstructed temperature evolution at the top of the Trigonodus Dolomit, based on data in Nagra (2002). See Fig. 1 for well locations. (For interpretation of the references to colour in this figure legend, the reader is referred to the Web version of this article.)

3. Tectonic evolution

The Swiss Molasse Basin is characterized by a rather complex tectonic evolution including two major cycles of burial and uplift (Fig. 2). Middle Triassic sedimentation of the Muschelkalk was followed by progressive burial due to lithospheric stretching and related subsidence of large parts of central Europe throughout most of the Jurassic and Cretaceous (Wildi et al., 1989; Ziegler, 1990; Loup, 1992). This sequence ended at a first phase of basin inversion in response to the onset of crustal shortening and finally the collision of the European and Adriatic plates during the Eocene–Oligocene (Pfiffner, 2014). Downwarping of the European plate during the Eocene–Middle Miocene created the North Alpine Foreland Basin and led to two cycles of shallow-marine and continental infill deposits (Pfiffner, 2014). The Swiss segment of the Basin is known as the Swiss Molasse Basin (SMB). In its NE sector, maximum burial occurred at ca. 10 Ma (Fig. 2; Mazurek et al., 2006), such that the basin sediments were on average 1090 m deeper than their present-day depths (Nagra, 2002). Late Miocene–-Pliocene (~10–3 Ma) thin-skinned Alpine shortening (Laubscher, 1961) resulted in a second phase of basin inversion, raising the Muschelkalk to its present-day depth. The thermal history of the sediments is shown in Fig. 2D.

4. Sampling and methods

4.1. Samples and maximum burial depths

Analyses have been performed on drill-core samples of the dolostones recovered from current depths of 58–2433 m from various wells across the Swiss Molasse Basin (Fig. 1; Table A.1 in appendix). Abbreviations of the well names (Fig. 1) are combined with the current depth to identify the samples (e.g. LIN 2258.14 indicates a sample from 2258.14 m depth in the Lindau well). The maximum burial depth of each sample has been reconstructed from published age–burial curves for the wells (e.g. Fig. 2; Nagra, 2002; Mazurek et al., 2006), yielding a range of 1148–3523 m for the studied set of samples (Table A.1 in appendix). Maximum burial depths (denoted z_{max}) are used throughout the remainder of this article. All of the analysed samples are free of macroscopic fractures.

4.2. Petrographic methods

Thin sections of 30 μm thickness were cut parallel to the depth-axis of the cores. Observations were made by transmitted light microscopy (Olympus BX51 polarizing microscope), UV-fluorescence microscopy (Olympus U-RFL-T mercury source 365 nm epi-illumination with BP 330–385 nm band-pass and BA420 barrier filters attached to a BX51 microscope) and scanning electron microscopy (Zeiss EVO®50).

In addition to thin-section petrography, stylolites have been characterized macroscopically following the approach of Tada and Siever (1989) and Ehrenberg (2006). Thus, the stylolites were classified as either “jagged” or “smooth”, and their amplitudes, thicknesses and frequencies were recorded.

4.3. Crystal size distributions

Crystal size distributions have been measured at various wells from various depths. The measurements were made on microphotographs of thin-sections viewed under plane- and crossed-polarized transmitted light. Depending on the crystal sizes, magnifications of 20–50x were used. The measurements were performed by digital image analysis using *ImageJ* (freeware obtainable at https://imagej.net/). To ensure statistical robustness (Morgan and Jerram, 2006), the sizes of 250 crystals were measured in each sample. The sizes were taken as equal to the longest axis of each crystal as viewed in 2D projection.

4.4. Pore sizes and shapes

The effect of increasing overburden on pore sizes and shapes is investigated by comparing samples from where the Trigonodus Dolomit underwent the least burial (Bözberg: z_{max} = 1148 m), with those from where it underwent the greatest burial (Lindau: z_{max} = 3315 m). Pore sizes and shapes were measured by processing SEM–backscattered electron (BSE) images using *ImageJ*. Image contrast and brightness were adjusted manually to clearly distinguish solid phases from pores. The images were then thresholded and compared with the original image to verify the processing. At each well a total of five samples showing mudstone fabrics and containing exclusively intercrystalline pore space were analysed. The BSE images were acquired at 70x magnification to capture large and medium pore sizes (pore cross-sections > 100 μm^2) and at 1000x magnification to capture small pore sizes (pore cross-sections < 100 μm^2). The 100 μm^2 cutoff is the pore size at which the resolution of the 70x magnification images (1.33 μm/pixel) is too low for accurate image processing. For each sample, 6–12 images at 70x magnification and 12–24 images at 1000x magnification were analysed.

Pore shapes were determined objectively by digitizing the pore perimeters according to the approach of Bakker and Diamond (2006), again using *ImageJ*. The "regularity" of each pore was calculated from the parameter (perimeter)^2/(4π·area), where value 1 (a circle) denotes "regular" and value 4 (a 4-pronged star) denotes "irregular". The "elongation" was determined from the length ratio of the major and minor axes of area-equivalent ellipses fitted to the measured area, where value 1 (a circle) denotes "equant" and value 10 (a stretched ellipse) denotes "elongate".

4.5. Petrophysical data

Petrophysical data on the Muschelkalk dolostones, including matrix porosity and matrix permeability, were obtained from laboratory analyses of drill core and from wireline geophysical logs. The porosity of the cores was measured at room temperature and pressure on 2.5 cm diameter plugs using a Micromeritics™ AccuPyc II 1340 helium gas displacement pycnometer. Pseudo-logs of matrix porosity were also calculated from density logs acquired at room temperature and pressure using a Geotek Multi-Sensor Core Logger (MSCL) with high spatial resolution (5 mm).

The permeability of the cores was measured at CoreLab Ltd. in Aberdeen, Scotland using an unsteady-state pressure decay permeameter (CMS™-300 Core Measurement System) at confining pressures greater than or equivalent to the down-hole lithostatic load minus the hydrostatic pressure (i.e. at pressures between 5.5 and 35.6 MPa). The results were corrected for the Klinkenberg effect.

The wireline log data include porosity logs deduced from lithodensity logs (LDL), compensated neutron logs (CNL) and sonic logs (DT) using the algorithms provided by Schlumberger (1989). The logs were screened for borehole roughness and breakouts. The laboratory core-measurements were used to calibrate the accepted log segments and to derive robust porosity and porosity–permeability correlations that are valid even for the wells without core.

5. Results

5.1. Rock fabrics and diagenesis

Our petrographic investigations show that ~80 vol% of all the available Upper Muschelkalk core sections (as listed in Table A.1) display mudstone fabrics, regardless of burial depth. The remaining ~20 vol% consist of bioclastic wackestones, packstones and grainstones composed largely of shell hashes, peloids and ooids. The Trigonodus Dolomit is essentially a monomineralic dolostone whereas the Dolomit der Anhydritgruppe is mineralogically variable, containing ≤48 wt% anhydrite, ≤ 32 wt% quartz, ≤ 51 wt% clay minerals and ≤42 wt% calcite (for references to these analyses see Table A.1).

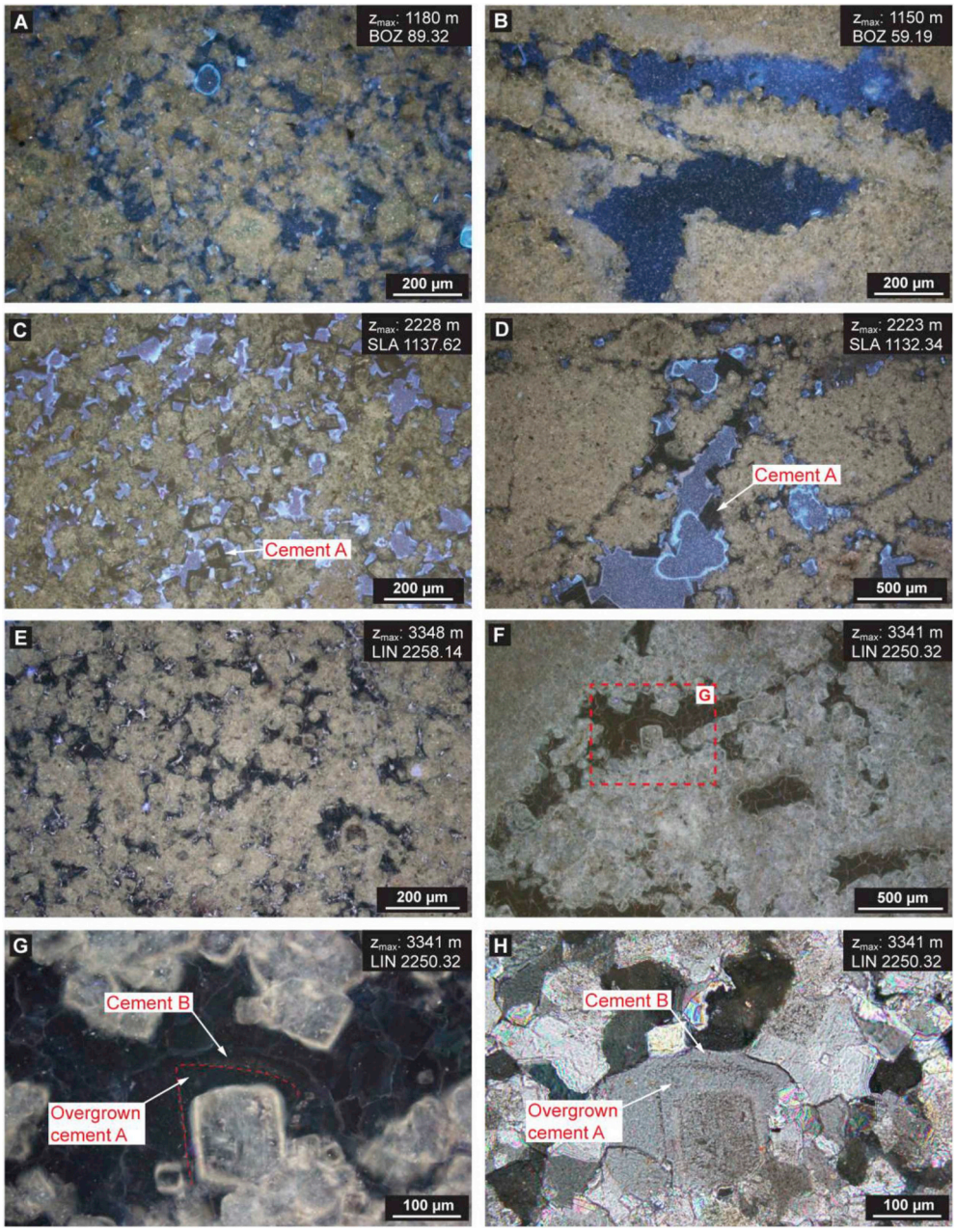

Fig. 3. Features of non-fluorescent dolomite cement as a function of maximum burial depth (z_{max}) in the Trigonodus Dolomit, Swiss Molasse Basin. At the Bözberg (BOZ) well, where burial was shallowest, precipitation of dolomite cement is not significant and has only marginally affected interparticle (A) and separate-vug porosity (B). Blue areas show UV-colour of epoxy and thus represent porosity. At intermediate burial depth interparticle (C) and separate-vug porosity (D) are partly cemented by non-fluorescent dolomite (cement A). However, the degree of cementation and associated porosity reduction is moderate and most of the pore space has remained open. (E–H) In the deeply buried Lindau well (LIN), dolomite cement A is present too, but is overgrown by later non-fluorescent dolomite (cement B), which fills a major portion of the available interparticle and separate-vug pore space (A–G: UV-fluorescence microscopy; H: crossed polarized, transmitted light microscopy). (For interpretation of the references to colour in this figure legend, the reader is referred to the Web version of this article.)

Several diagenetic processes have affected the porosity and permeability of the original carbonates. Dolomitization of the Trigonodus Dolomit is known to have occurred via early diagenetic seepage reflux at depths of at most 40 m (Schauer and Aigner, 1997; Adams and Diamond, 2018; Adams et al., 2018) and it proceeded in a mainly fabric-destructive manner. Overdolomitization is very weak, as demonstrated by the paucity of dolomite cements in the interparticle and separate-vug pore space in samples from the shallow wells that are least affected by compaction (especially chemical compaction; Fig. 3A and B). Generally, there is a lack of evidence for any extensive early diagenetic cementation in the Trigonodus Dolomit (Adams et al., 2018). Dissolution of bivalve shell fragments during dolomitization created shell-mouldic porosity, and late-diagenetic (Neogene) dissolution of anhydrite nodules created anhydrite-mouldic porosity.

At intermediate burial depths (z_{max} = 1890–2290 m), interparticle and separate-vug pores are partly cemented by a non-fluorescent dolomite cement (cement A in Fig. 3C and D). The degree of cementation and associated porosity reduction is moderate and most of the pore space remained open (Fig. 3C and D).

Under deep burial ($z_{max} \geq$ 3090 m) the above-mentioned dolomite cement is still present, but it is overgrown by a later generation of similarly non-fluorescent dolomite cement (Fig. 3E–H; cement B in Fig. 3G and H), which fills much of the available interparticle and separate-vug pore space. Individual crystals of this late-stage dolomite cement usually show saddle habit (curved crystal faces) and undulose optical extinction (Fig. 4A–C). Some of the crystals show growth zonation: the original BSE-dark crystal cores (marked by clouds of primary fluid inclusions) are mantled by BSE-bright, weakly Fe-enriched saddle dolomite filling the intercrystalline pore space (Fig. 4D). No evidence for pressure solution was found between saddle dolomite crystals.

5.2. Petrographic evidence of compaction with increasing depth

Petrographic evidence for mechanical compaction is visible mainly in oolites, where convexo-concave grain contacts between individual

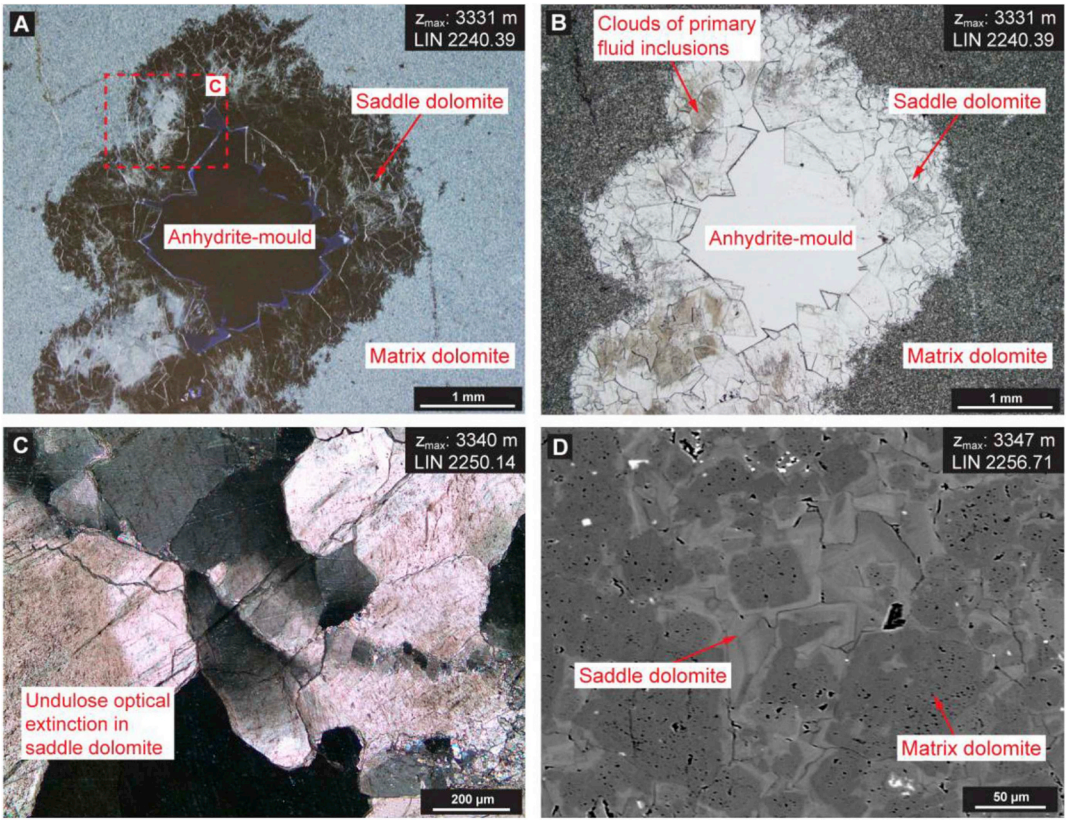

Fig. 4. Textures and relative timing of cement in the Trigonodus Dolomit in the deep well of Lindau. Values of z_{max} indicate maximum burial depth. (A) Non-fluorescing saddle dolomite within separate-vug porosity (anhydrite-mould). (B) Individual dolomite crystals often show curved crystal faces, high abundances of primary fluid inclusions (dark specks) and (C) undulose extinction. (D) BSE-bright, weakly Fe-enriched saddle dolomite overgrowing BSE-dark matrix dolomite and filling intercrystalline pore space. Dark specks within crystals of matrix dolomite are breached primary fluid inclusions. Bright dots are pyrite (A: UV-fluorescence microscopy; B: plane polarized, transmitted light microscopy; C: crossed polarized, transmitted light microscopy; D: SEM-BSE image).

ooids indicate plastic deformation (Fig. 5A). In the mudstone fabrics, the only direct evidence for mechanical compaction is the very fine splinters of dolomite in pores between larger crystals (Fig. 5B). These are present only in the well that underwent the least burial (Bözberg: z_{max} = 1148 m).

Evidence for chemical compaction via pressure-solution is found in the abundant stylolites, which predominantly occur in marly interlayers within the dolostones in all wells at all depths. Two genetic types of stylolites are present within the Upper Muschelkalk dolostones: (1) common bedding-parallel diagenetic stylolites (either jagged or smooth; Fig. 5C and D) formed as a result of the vertical stress induced by the overburden and (2) less common, steeply dipping tectonic stylolites (Fig. 5E) formed as a result of horizontal, compressive stresses.

Fig. 6 compares the characteristics of diagenetic stylolites as a function of maximum burial depth in several wells. The frequency of stylolites increases from 3.4/m in the Bözberg well, which provides the shallowest data, to 9.4/m in the deep Lindau well (Fig. 6), such that the total thickness of the dissolution seams increases with depth. In addition, the average amplitude of jagged stylolites increases with depth from 1.3 mm at Bözberg to 2.4 mm at Lindau.

Tectonic stylolites usually display jagged texture with amplitudes of up to 8 mm. Mineralogically the stylolites consist of 10–20 wt% organic carbon, the remainder being pyrite, quartz and 10 Å phyllosilicates, presumably clays.

5.3. Crystal size distributions and crystal textures

Fig. 7 shows the average sizes of dolomite crystals in the Trigonodus Dolomit at various wells as a function of the distance of the samples from the base of the unit. Independently of the depth of the Trigonodus Dolomit, each well shows a similar trend in crystal size distribution. Thus, crystal sizes are on average ~10 µm at the top of the unit and they steadily increase towards the base where average crystal sizes reach ~40 µm. This size distribution does not result from burial diagenesis or compaction but rather is inherited from the original dolomitization event at depths less than 40 m (Adams et al., 2018). To avoid any confusion with this pre-burial variation in crystal sizes, we have confined our investigation of the effects of increasing overburden to mudstone samples from the coarsely crystalline lowermost 10 m of the Trignodus Dolomit unit at each well.

Possible effects of increasing overburden on dolomite textures include crystal breakage by mechanical compaction and modification of the crystal texture by intercrystalline pressure solution. Fig. 8 illustrates how the textures of the rock-forming dolomite crystals in the Trigonodus Dolomit change with increasing depth of maximum burial. At the shallowest level sampled (z_{max} = 1185 m) the rock matrix is composed of a relatively “loose” framework of euhedral dolomite crystals and considerable amounts of intercrystalline pore space (Fig. 8A and B). Evidence for intercrystalline pressure solution is rare and individual crystals do not show severe breakage. At z_{max} = 1930 m the rock matrix consists of a denser packing of predominantly subhedral dolomite crystals with distinctly less intercrystalline pore space (Fig. 8C). Crystal–crystal contacts are commonly straight, but curved, lobate, serrated and sutured boundaries are present too (Fig. 8D). Crystal breakage is generally rare. At z_{max} = 2230 m the intercrystalline pore space is further decreased (Fig. 8E) and crystal–crystal contacts become increasingly irregular (Fig. 8F). Finally, at z_{max} = 3347 m, the rock matrix consists of tightly interlocked, anhedral dolomite crystals and it contains few intercrystalline pores (Fig. 8G). The crystal boundaries are commonly curved, lobate, serrated, sutured or otherwise irregular and

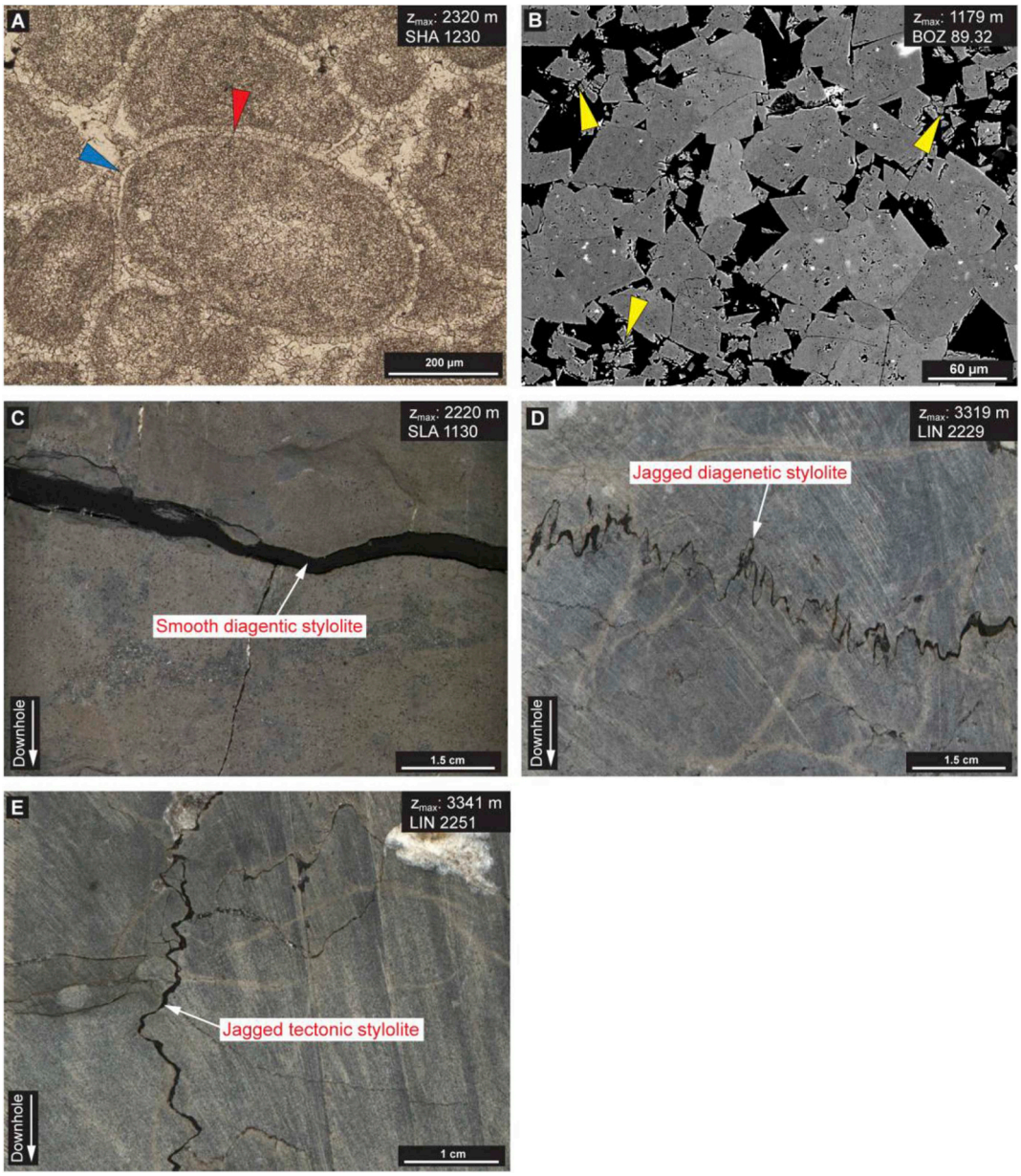

Fig. 5. Compaction features in the Muschelkalk dolomites. Values of z_{max} indicate maximum burial depth. (A) Convexo-concave grain boundary (red arrow) in oolites and detachment of cement rims (blue arrows) indicative of plastic deformation and associated mechanical compaction. (B) In mudstone fabrics, the only direct evidence for mechanical compaction is fine splinters of dolomite in the intercrystalline pore space (yellow arrows). Pressure-solution features include (C) "smooth" and (D) "jagged" diagenetic stylolites, as well as (E) tectonic stylolites with "jagged" texture (A: plane polarized, transmitted light microscopy; B: SEM-BSE image; C–E: reflected-light photograph of halved drill core). (For interpretation of the references to colour in this figure legend, the reader is referred to the Web version of this article.)

individual crystals penetrate each other and show truncations and indentations (Fig. 8H). Again, there is no evidence of major crystal breakage by mechanical compaction.

5.4. Pore sizes and pore geometry

Table 1 shows that the 2D porosity calculated from digital image analyses generally fits well with the porosity determined by helium-pycnometry on the corresponding plug samples. The cross-sectional areas of the pores are therefore good representations of their volumes.

In order to investigate the effect of increasing overburden on pore sizes in the Trigonodus Dolomit mudstones, Fig. 9 compares the distribution of pore sizes in samples that underwent the least burial (Bözberg: z_{max} = 1148 m) with those that underwent the greatest burial (Lindau: z_{max} = 3315 m). The comparison is made between samples from the relatively coarsely-crystallized, lowermost 10 m of the unit at both wells. The quantity and distribution of pore cross-sections < 100 µm^2 do not differ significantly with burial depth. However, the quantity of pores larger than 100 µm^2 is markedly different between the two wells. At Bözberg, considerable amounts of pores larger than 100 µm^2 are present and they constitute between 40 and 92% of the total 2D pore space of the rock (Table 1). In contrast, at the deep well of Lindau the quantity of pores larger than 100 µm^2 is minor (1–11% of the total 2D pore space; Table 1).

In addition to the above differences in pore sizes, there are distinct differences in the pore shapes at the two wells (Fig. 10). For better visualization the data are illustrated as average values of "irregularity" and "elongation" for specific pore size intervals (see Section 4.3 for

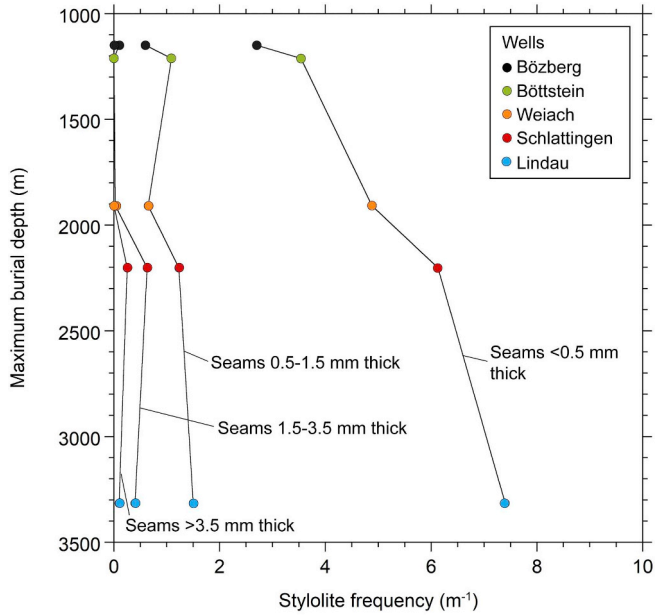

Fig. 6. Frequency and thickness of diagenetic stylolites in the Tridonodus Dolomit as a function of maximum burial depth in various wells. Stylolite seams are grouped into four thickness intervals shown by the four curves. Both frequency and thickness of the seams increase with increasing depth.

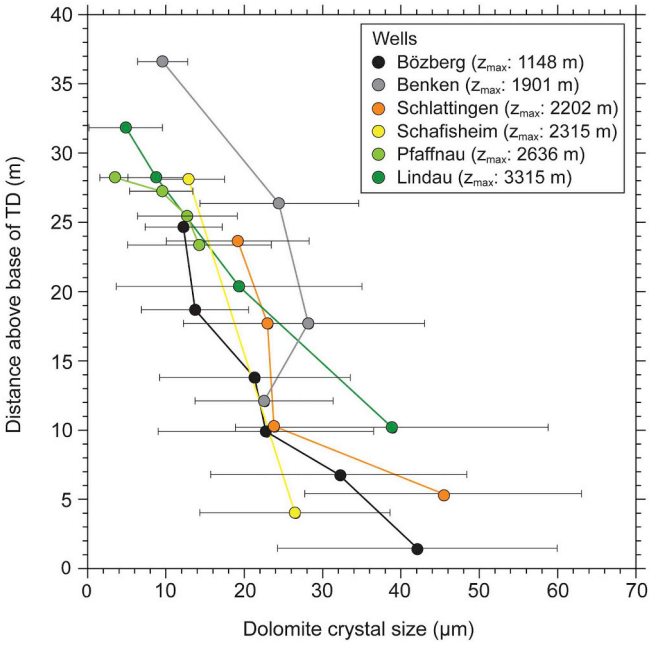

Fig. 7. Dolomite crystal size distribution within the Trigonodus Dolomit (TD) at various wells, inherited from the pre-burial dolomitization event. Values of z_{max} denote maximum burial depth. Averages (dots) and ranges ($\pm 1\sigma$) of crystal sizes are shown as a function of vertical distance above the base of the Trigonodus Dolomit (i.e. above the contact with the Hauptmuschelkalk).

definitions and Fig. 10 for example shapes). Where the least burial occurred (Bözberg) all the pores are nearly equant, regardless of size. Where the deepest burial occurred (Lindau), pores with cross-sections below 100 μm^2 are nearly equant too, whereas larger pores are increasingly elongated. No preferred orientation was observed in the axes of elongation (i.e. there is no flattening due to the overburden). The irregularity of the pores at Lindau is almost the same as that at Bözberg.

5.5. Porosity–depth curves

Tables A.1 and A.2 list all the wells at which drill core (11 wells) and wireline log data (15 wells) were used to deduce matrix porosity. Fig. 11A and B and Tables 2 and 3 show average values of matrix porosity in the dolostones as a function of their maximum burial depths (Section 3). The illustrated best-fit porosity–depth curve for the Trigonodus Dolomit is an exponential regression. Thus, porosity decreases rapidly within the first 1.5 km below surface (from 40–45 to 17–19 vol %). At depths of more than 3000 m, porosity maintains consistently low values of 2–8 vol%. The Dolomit der Anhydritgruppe shows a similar evolution of porosity with depth, but the scatter of the data is much larger and hence the correlation with depth is rather poor.

5.6. Permeability–depth curves

Permeability was determined based on the same drill cores (11 wells) and wireline logs (15 wells) as used for the porosity determinations (Tables A.1 and A.2). Fig. 12A and B and Tables 4 and 5 show the matrix permeability of the dolostones as a function of their maximum burial depths (Section 3). Geometric averages are plotted according to Warren and Price (1961). The matrix permeability of the Trigonodus Dolomit decreases from 90 to 120 to ~1 mD within the first 1.5 km of overburden and finally reaches values of less than 0.01 mD at depths greater than 3000 m. The DAG shows a similar depth trend but as its permeability has been calculated from the scattered porosity measurements (Section 5.5), the correlation with depth is poor.

6. Discussion

6.1. Representativeness of laboratory and wireline log measurements for buried rocks

The porosity–depth curves in Figs. 11 and 12 implicitly assume that the laboratory measurements of porosity reported above are representative of the rock porosity at maximum burial depths. This assumption is justified for the present sample set by two arguments. First, the measured samples were carefully selected to be absolutely free of macroscopic fractures. Therefore, no readjustment of fracture dimensions upon retrieval of the core from depth could have influenced the porosity measurements. Second, only a trivial amount of elastic volume change occurs upon release of the lithostatic load during coring and retrieval from the well to laboratory conditions. This can be illustrated for the deepest sample retrieved from the Entlebuch well at ~5000 m depth, where the temperature was ~100 °C. As the measured dolostones are texturally isotropic, the elastic relaxation of the bulk rock can be calculated from the equation-of-state for dolomite in Berman (1988). Using an average rock density of 2.5 g/cm^3 for the sediments in the Swiss Molasse Basin, the 5000 m overburden corresponds to 123 MPa lithostatic confining pressure. Therefore, as the sample decompresses from 123 to 0.1 MPa, it expands by 10^{-3} vol%, which is negligible compared to the uncertainty of the laboratory porosity measurements. Decompression from maximum burial (6100 m = 150 MPa at ~120 °C) yields a similarly negligible value of 10^{-2} vol%.

In contrast to the porosity measurements, the permeability of the plugs was measured under high confining pressure at room temperature (Section 4.4), hence the reported values may be slight underestimates due to failure to account for thermal contraction of pore throats.

A further point regarding representativeness is our use of digital image processing of 2D images to estimate pore sizes. No preferred orientation of elongate pores was found in any of the samples, not even in those from the deep Lindau well where flattening of pores due to the high overburden could have been expected. The porosity in the studied dolostones therefore appears to be texturally isotropic, as confirmed by

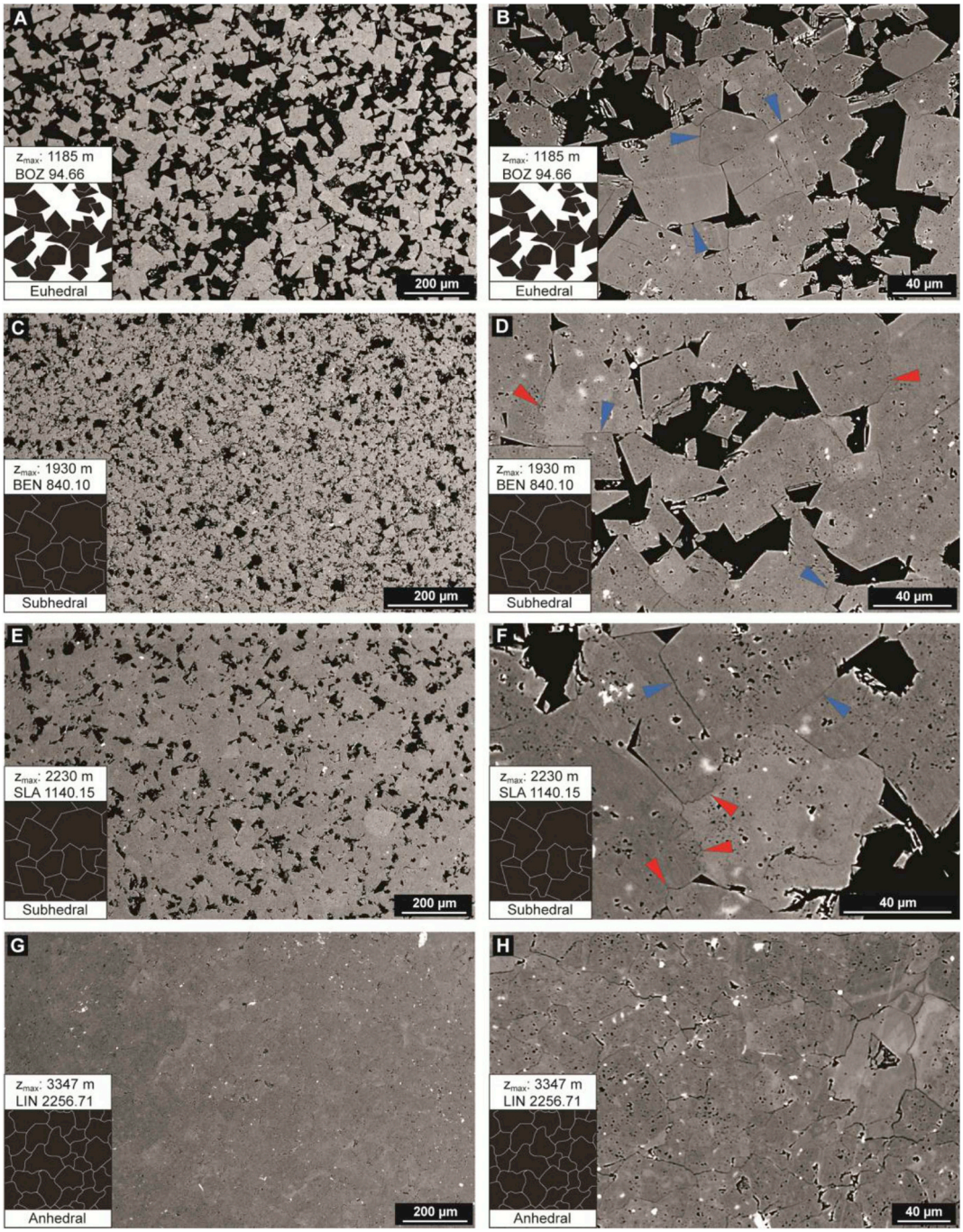

Fig. 8. Textures of matrix dolomite as a function of maximum burial depth (SEM-BSE images). All samples are from the relatively coarsely-crystallized lowermost 10 m of the Trigonodus Dolomit. Values of z_{max} indicate maximum burial depth. Black dots within crystals are primary fluid inclusions breached by cutting and polishing the samples. Bright dots are pyrite. Insets in the lower left corner of the images show the classification scheme of dolomite crystal textures combined from Gregg and Sibley (1984) and Sibley and Gregg (1987) in Machel (2004). (A) In samples that underwent the least burial (z_{max} = 1185 m) the rock matrix is a loose network of euhedral dolomite crystals with considerable intercrystalline pore space. (B) Crystal faces and boundaries are generally straight and euhedral (blue arrows). (C) At z_{max} = 1930 m the rock matrix shows denser packing of subhedral crystals and contains less intercrystalline pores. (D) Crystal boundaries are mostly straight (blue arrows) but curved, lobate, serrated and sutured boundaries are present too (red arrows). (E) Further decrease of intercrystalline porosity at z_{max} = 2230 m and (F) increasingly irregular dolomite crystal-crystal contacts (red arrows). (G) At z_{max} = 3346 m the rock matrix shows dense packing of anhedral dolomite crystals and contains few intercrystalline pores. (H) Crystal boundaries are commonly curved, lobate, serrated, sutured or otherwise irregularly shaped. Bright zones are saddle dolomite cement (cf. Fig. 4B). (For interpretation of the references to colour in this figure legend, the reader is referred to the Web version of this article.)

the good match between 2D digital image analyses and 3D helium-pycnometry results (Table 1).

In the Trigonodus Dolomit, the drill core data (MSCL-porosity) can be best reproduced by the wireline LDL-porosity (error of prediction $2\sigma_{est}$ = ± 3.3 vol%), followed by CNL-porosity ($2\sigma_{est}$ = ± 4.3 vol%) and finally DT-porosity ($2\sigma_{est}$ = ± 5.2 vol%). This trend of reproducibility also applies to the Dolomit der Anhydritgruppe, however, the errors of prediction are distinctly larger (LDL: ± 4.6 vol%; CNL: ± 6.8 vol%; DT: ± 10.7 vol%) owing to variations in the mineralogical composition of the Dolomit der Anhydritgruppe (Section 5.1),

Table 1
Porosity determined by digital image analysis (DIA) compared to porosity measurements of plug samples by helium pycnometry.

Sample	DIA porosity[a]: pores < 100 μm² (vol %)	DIA porosity[a]: pores > 100 μm² (vol%)	Total DIA porosity[a] (vol %)	Plug porosity[b] (vol%)	Difference (Plug-DIA) (vol %)
BOZ 94.66 M	7.36	4.86	12.22	12.31	+0.09
BOZ 94.66 S	2.30	28.28	30.58	29.32	−1.26
BOZ 77.40	7.13	11.00	18.13	18.20	+0.07
BOZ 71.40	9.96	13.32	23.28	23.80	+0.52
BOZ 89.32	3.15	13.51	16.66	19.80	+3.14
LIN 2228.65	1.54	0.20	1.74	1.70	−0.04
LIN 2235.19	1.99	0.17	2.16	1.80	−0.36
LIN 2238.78	1.19	0.04	1.23	1.50	+0.27
LIN 2246.67	1.23	0.10	1.33	1.30	−0.03
LIN 2256.71	1.39	0.02	1.41	1.20	−0.21

The uncertainties of the porosity derived from DIA depends on the image processing and theresholding and thus cannot be quantified. However, the excellent match between DIA porosity and He-Porosity idicates that it is not substantial.
[a] No uncertainties quantifiable.
[b] Uncertainty = 0.01–0.1 vol% (1sd).

which bias the porosity calculated from both the wireline and drill core logs. As a consequence, the porosity data for the Dolomit der Anhydritgruppe scatter widely (cf. Figs. 11B and 12B) and they only roughly define a porosity–depth trend. Thus, they constitute a poor basis to decipher compaction processes. We therefore confine the following discussions to the Trigonodus Dolomit, which owing to its

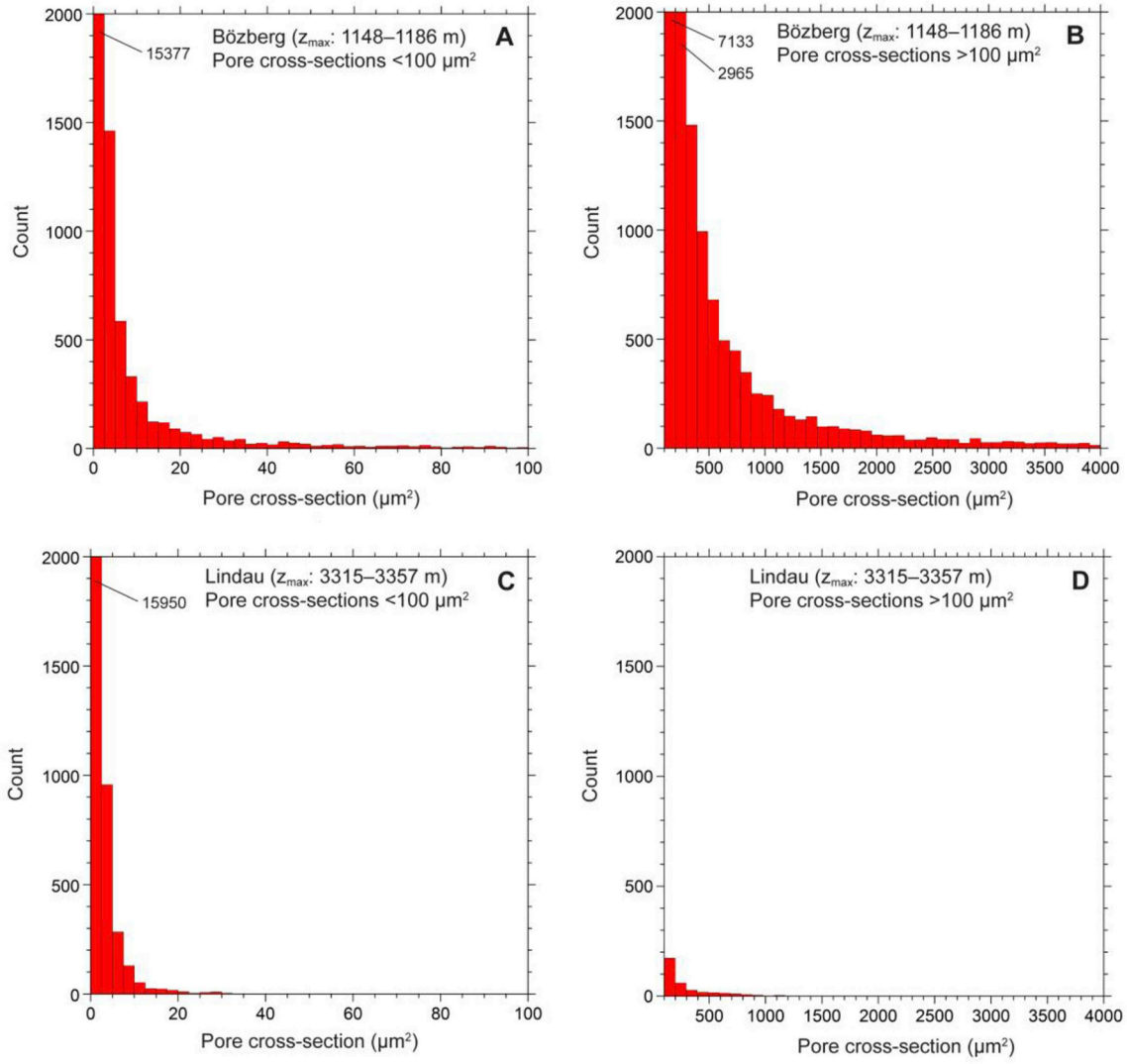

Fig. 9. Pore-size distribution in samples of the Trigonodus Dolomit that underwent the least burial (Bözberg: z_{max} = 1148–1186 m) compared those that underwent the greatest burial (Lindau: z_{max} = 3315–3357 m). All samples are texturally mudstones from the relatively coarsely-crystallized lowermost 10 m of the Trigonodus Dolomit. Values of z_{max} indicate maximum burial depth. (A and C) Pore sizes < 100 μm². (B and D) Pore sizes > 100 μm². Values in upper left corners indicate off-scale frequencies.

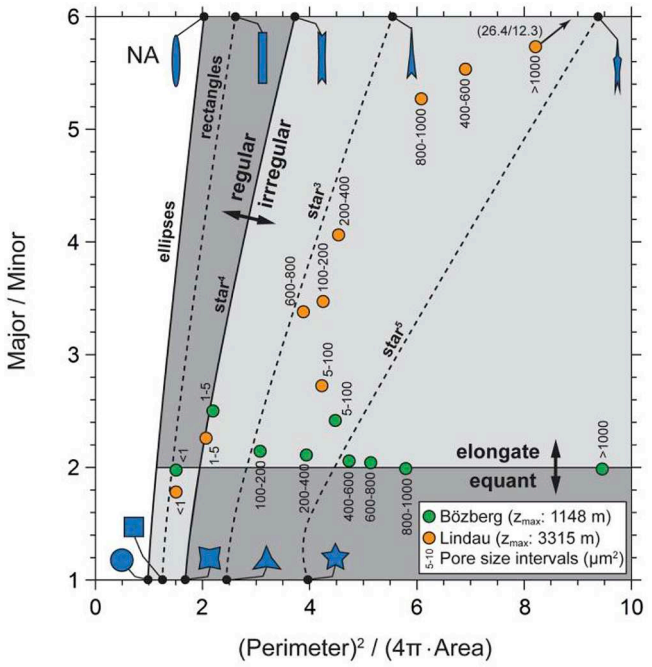

Fig. 10. Shapes of pores in the Trigonodus Dolomit at the Bözberg (BOZ) and Lindau (LIN) wells determined by digital image analysis according to the method of Bakker and Diamond (2006) (see section 4.3 for explanation). At the shallow Bözberg well all pores have nearly equant geometries, regardless of size. At the deep Lindau well, pores < 100 µm^2 are nearly equant whereas larger pores are increasingly elongated. The irregularity of pores at Lindau is almost the same as that at Bözberg. Values of z_{max} indicate maximum burial depth.

monomineralic composition has yielded distinctly higher-quality porosity and permeability data.

6.2. Porosity–depth curves

The dolomitization of the Trigonodus Dolomit is known to have occurred via early diagenetic seepage reflux at depths of at most 40 m (section 5.1). Extrapolation of the empirical curve in Fig. 11A to 40 m depth suggests that the dolostone initially had a porosity of around 40–45 vol%, although values between 30 and 50 vol% are possible. The question of interest is how its porosity decreased to values as low as 2–8 vol% upon 3500 m of burial.

The presence of diagenetic stylolites at the well of Bözberg, where the Muschelkalk was buried to a maximum depth of ~1185 m, indicates that pressure solution has thinned the formation to a certain extent at these depths. However, Fig. 8A shows that the rock matrix of the Trigonodus Dolomit between the stylolites is composed of a relatively loose framework of euhedral dolomite crystals and considerable intercrystalline pore space (18–29 vol% plug porosity, Table 1). Since crystal-crystal contacts are relatively limited in this texture, moderate amounts of pressure solution cannot close large intercrystalline pores. We therefore conclude that mechanical compaction by crystal rearrangement and minor crystal breakage are the dominant porosity-reducing mechanisms at these depths. These mechanisms have affected large pores more strongly than small pores (Fig. 10), presumably because the walls of large pores have proportionally less support from the surrounding rock matrix than small pores.

At the Benken well, where the Muschelkalk was buried to a maximum depth of ~1930 m, the individual dolomite crystals are interlocked and distinctly less intercrystalline pore space is present (Fig. 8C and D). The interlocking of the predominantly subhedral crystals inhibits rearrangement of crystals and thus, if mechanical compaction had occurred, it must have proceeded via crystal breakage. However,

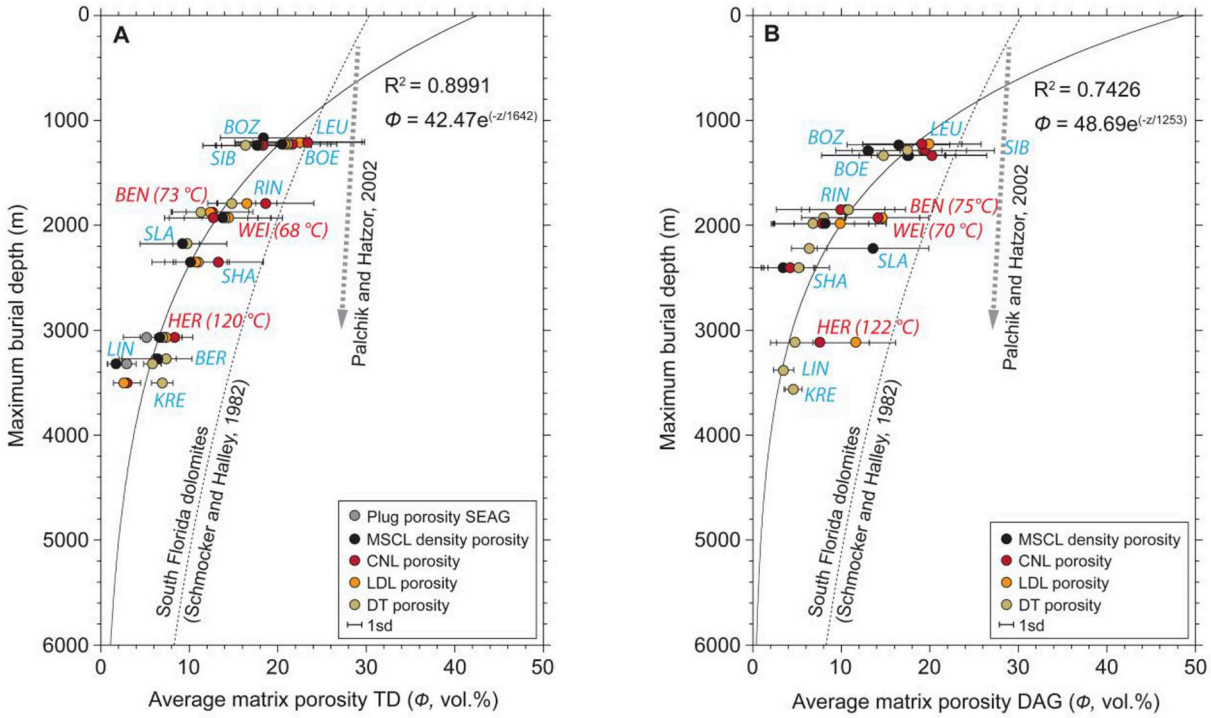

Fig. 11. Porosity–depth trends of (A) the Trigonodus Dolomit (TD) and (B) the Dolomit der Anhydritgruppe (DAG) according to several methods (see text). The depth corresponds to Miocene maximum burial (Fig. 2), which in the NE Swiss Molasse Basin was on average 1090 m deeper than the present-day depth. Temperatures at the wells of Benken, Weiach and Herdern (red) represent temperatures during Miocene maximum burial calculated by basin modelling (Nagra, 2002; Mazurek et al., 2006). (For interpretation of the references to colour in this figure legend, the reader is referred to the Web version of this article.)

Table 2
Average matrix porosity in the Trigonodus Dolomit for the various wells across the Swiss Molasse Basin calculated from wireline logs, core-scanner density logs (MSCL) and plug measurements. Uncertainties represent one standard deviation.

Well	Present-day depth[a] (m)	Maximum burial[b] (m)	MSCL poro[c] (vol%)	CNL poro[d] (vol%)	LDL poro[e] (vol%)	DT poro[f] (vol%)	Plug poro SEAG[g] (vol%)
Benken	830	~1880	–	12.57 ± 4.64	12.42 ± 4.32	11.32 ± 1.67	–
Berlingen	2185	~3270	6.34 ± 3.96	–	–	7.39 ± 1.13	6.16 ± 4.13
Böttstein	136	~1230	20.78 ± 5.19	21.60 ± 5.06	20.96 ± 3.88	21.51 ± 4.09	–
Bözberg	77	~1170	18.34 ± 4.84	–	–	–	–
Entlebuch	5066	–	–	4.09 ± 2.02	4.33 ± 2.31	–	0.79 ± 0.66
Herdern	2006	~3070	6.67 ± 2.22	8.36 ± 2.05	7.37 ± 1.83	6.93 ± 0.83	5.16 ± 2.60
Kreuzlingen	2424	~3500	2.94 ± 1.53	–	–	6.93 ± 1.21	2.49 ± 1.03
Leuggern	53	~1210	–	23.35 ± 6.16	22.49 ± 7.31	–	–
Lindau	2246	~3320	1.70 ± 0.99	–	–	5.86 ± 1.02	2.92 ± 1.06
Pfaffnau	1561	–	8.02 ± 3.13	–	–	9.58 ± 1.71	8.13 ± 3.33
Riniken	634	~1790	–	18.63 ± 5.44	16.50 ± 3.41	14.79 ± 2.70	–
Schafisheim	1242	~2350	10.15 ± 4.35	13.27 ± 5.05	10.75 ± 3.51	10.95 ± 2.48	–
Schlattingen	1129	~2170	9.33 ± 4.89	–	–	9.65 ± 1.49	–
Siblingen	192	~1240	17.65 ± 6.15	18.30 ± 4.68	17.74 ± 4.78	16.34 ± 3.41	–
Treycovagnes	2538	–	–	6.57 ± 4.23	3.51 ± 2.25	7.30 ± 3.86	–
Weiach	838	~1930	13.87 ± 6.67	12.76 ± 5.05	14.35 ± 4.92	14.03 ± 2.59	–

[a] Average depth.
[b] Average depth at Miocene maximum burial according to studies by Nagra (2002) and Mazurek et al. (2006).
[c] MSCL: Multi-Sensor Core Logger.
[d] CNL poro: Porosity deduced from wireline neutron log.
[e] LDL poro: Porosity deduced from wireline density logs.
[f] DT poro: Porosity deduced from wireline sonic logs.
[g] SEAG: Corporation for Swiss Petroleum.

neither at Benken, nor at the deeper wells of Schlattingen and Lindau is there unequivocal evidence for this process (Fig. 8C–H). It seems more likely that, at depths between ~1185 and ~1930 m, there is a transition from dominantly mechanical compaction to pure chemical compaction via pressure solution. The sutured crystal–crystal contacts in Benken and Schlattingen wells (Fig. 8D and F), for example, are direct evidence of interparticle pressure solution. The transition between mechanisms takes place where average matrix porosities are ~13–20 vol%. This conclusion contrasts markedly with the experiments of Palchik and Hatzor (2002), who found that mudstone dolostones from ≤300 m depth with initial porosities of 5–29 vol% underwent no appreciable compaction upon loading to an equivalent depth of 3000 m (dashed arrow in Fig. 11A). This contrast implies that either the different sets of dolostones have very different mechanical properties or that the present study has failed to notice subtle evidence for significant pressure solution at depths shallower than ~1185–1930 m. In the absence of detailed descriptions of the experimentally tested rocks in Palchik and Hatzor (2002), it is unclear whether they can be directly compared to the Trigonodus Dolomit.

At the deep well of Lindau, where the Muschelkalk was buried to a maximum depth of ~3315 m, the rock matrix consists of densely packed anhedral dolomite crystals with deeply sutured and highly irregular intercrystal contacts reminiscent of stylolite shapes and it contains few intercrystalline pores (1.2–1.8 vol% total plug porosity, Table 1; Fig. 8G and H). The overall size of the individual crystals is largely preserved with increasing burial depth (Fig. 7), thus the loss in porosity is best viewed as an increase in closeness of crystal packing, facilitated by the anhedral crystal shapes (cf. Fig. 8A and G). In

Table 3
Average matrix porosity in the Dolomit der Anhydritgruppe for the various wells across the Swiss Molasse Basin calculated from wireline logs and core-scanner (MSCL) density logs. Uncertainties represent one standard deviation.

Well	Present-day depth[a] (m)	Maximum burial[b] (m)	MSCL poro[c] (vol%)	CNL poro[d] (vol%)	LDL poro[e] (vol%)	DT poro[f] (vol%)
Benken	880	~1930	–	14.15 ± 5.77	14.68 ± 4.21	8.01 ± 2.51
Berlingen	2251	–	–	–	–	–
Böttstein	201	~1330	14.75 ± 6.97	20.24 ± 6.20	17.58 ± 4.21	17.49 ± 5.45
Bözberg	143	~1230	16.46 ± 5.80	–	–	–
Entlebuch	5066	–	–	4.09 ± 2.02	4.33 ± 2.31	4.73 ± 2.08
Herdern	2057	~3120	–	7.56 ± 5.57	11.62 ± 4.53	4.73 ± 2.08
Kreuzlingen	2486	~3560	–	–	–	4.60 ± 0.94
Leuggern	94	~1250	–	19.11 ± 6.70	19.86 ± 3.79	–
Lindau	2291	~3380	–	–	–	3.46 ± 1.14
Pfaffnau	1616	–	–	–	–	11.61 ± 4.13
Riniken	694	~1850	–	9.94 ± 7.29	10.64 ± 4.25	10.77 ± 5.28
Schafisheim	1296	~2400	3.42 ± 3.51	4.18 ± 2.91	3.39 ± 2.39	5.20 ± 3.46
Schlattingen	1174	~2220	13.68 ± 6.30	–	–	6.37 ± 2.01
Siblingen	242	~1290	19.27 ± 8.02	19.47 ± 4.69	17.50 ± 3.88	12.98 ± 3.62
Treycovagnes	2593	–	–	4.35 ± 0.80	8.05 ± 0.82	2.30 ± 0.52
Weiach	893	~1980	8.11 ± 5.75	7.78 ± 5.30	9.86 ± 5.16	6.79 ± 4.69

[a] Average depth.
[b] Average depth at Miocene maximum burial according to studies by Nagra (2002) and Mazurek et al. (2006).
[c] MSCL: Multi-Sensor Core Logger.
[d] CNL poro: Porosity deduced from wireline neutron log.
[e] LDL poro: Porosity deduced from wireline density logs.
[f] DT poro: Porosity deduced from wireline sonic logs.

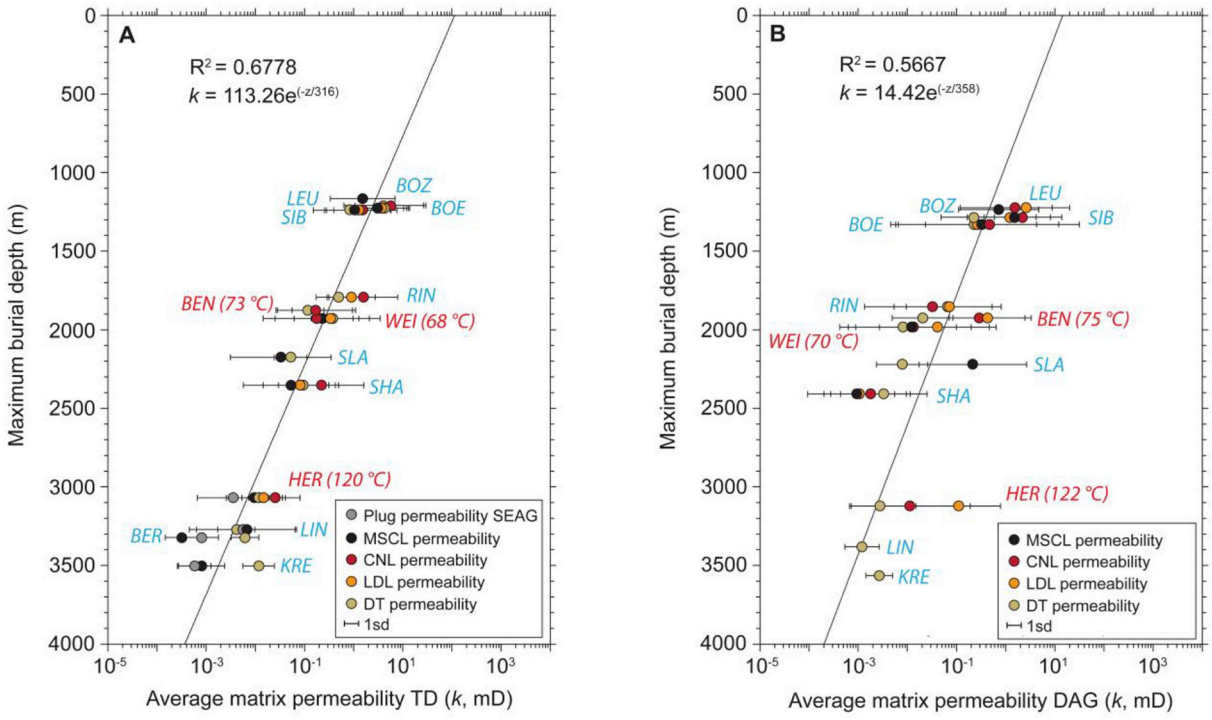

Fig. 12. Permeability–depth trends of (A) the Trigonodus Dolomit (TD) and (B) the Dolomit der Anhydritgruppe (DAG), according to several methods (see text). Permeability values represent geometric means; the depth corresponds to Miocene maximum burial (Fig. 2), which in the NE Swiss Molasse Basin was on average 1090 m deeper than the present-day depth. Temperatures at the wells of Benken, Weiach and Herdern represent temperatures during Miocene maximum burial calculated by basin modelling (Nagra, 2002; Mazurek et al., 2006).

Table 4
Average matrix permeability in the Trigonodus Dolomit for the investigated wells across the Swiss Molasse Basin calculated from the various porosity logs, as well as from plug porosities (data from SEAG) and based on the correlation between porosity and permeability. The errors correspond to one standard deviation (MSCL: Multi-Sensor Core Logger; SEAG: Corporation for Swiss Petroleum).

Well	Present-day depth[a] (m)	Maximum burial[b] (m)	Log k_{MSCL} (mD)	Log k_{NPHI} (mD)	Log k_{RHOB} (mD)	Log k_{DT} (mD)	Log k_{SEAG} (mD)
Benken	830	~1880	–	−0.77 ± 0.81	−0.79 ± 0.77	−0.93 ± 0.33	–
Berlingen	2185	~3270	−2.19 ± 1.00	–	–	−2.38 ± 0.38	−2.25 ± 1.09
Böttstein	136	~1230	0.49 ± 0.62	0.60 ± 0.54	0.55 ± 0.47	0.61 ± 0.47	–
Bözberg	77	~1170	0.18 ± 0.66	–	–	–	–
Entlebuch	5066	–	–	−2.77 ± 0.58	−2.69 ± 0.67	–	−3.82 ± 0.24
Herdern	2006	~3070	−2.02 ± 0.57	−1.59 ± 0.50	−1.83 ± 0.44	−1.92 ± 0.21	−2.45 ± 0.73
Kreuzlingen	2424	~3500	−3.10 ± 0.48	–	–	−1.93 ± 0.32	−3.23 ± 0.33
Leuggern	53	~1210	–	0.75 ± 0.72	0.61 ± 0.81	–	–
Lindau	2246	~3320	−3.50 ± 0.33	–	–	−2.21 ± 0.28	−3.09 ± 0.34
Pfaffnau	1561	–	−1.71 ± 0.72	–	–	−1.30 ± 0.38	−1.69 ± 0.73
Riniken	634	~1790	–	0.20 ± 0.70	−0.05 ± 0.49	−0.31 ± 0.45	–
Schafisheim	1242	~2350	−1.27 ± 0.97	−0.66 ± 0.87	−1.10 ± 0.73	−1.02 ± 0.51	–
Schlattingen	1129	~2170	−1.48 ± 1.02	–	–	−1.28 ± 0.33	–
Siblingen	192	~1240	0.03 ± 0.85	0.18 ± 0.58	0.10 ± 0.65	−0.07 ± 0.52	–
Treycovagnes	2538	–	–	−2.13 ± 1.01	−2.94 ± 0.65	−1.93 ± 0.97	–
Weiach	838	~1930	−0.65 ± 1.19	−0.75 ± 0.85	−0.45 ± 0.76	−0.43 ± 0.43	–

[a] Average depth.
[b] Average depth at Miocene maximum burial according to studies by Nagra (2002) and Mazurek et al. (2006).

contrast, maintenance of euhedral shapes would preclude close packing and thereby automatically preserve high porosity within the crystal aggregate.

Similar textures to those at Lindau have been observed in the Middle Devonian Alpena carbonates in the Michigan Basin (1500 m depth), including anhedral crystals with sutured and curved intercrystal contacts (Buxton and Sibley, 1981). The corresponding textures are called "fitted" fabrics and their importance as a major category of pressure solution features was recognized by Logan and Semeniuk (1976). Accordingly, the transition from euhedral textures at shallow depths to subhedral textures at intermediate depths to finally anhedral textures under deep burial (Fig. 8) is interpreted to reflect increasing chemical compaction with depth. This behaviour is further evidenced by the documented increase in abundance, width and amplitude of diagenetic stylolites with depth (Fig. 6).

In addition to diagenetic stylolites formed due to vertical stresses induced by the overburden, the Trigonodus Dolomit is also traversed by tectonic stylolites, which formed in response to Paleogene–recent convergence of the Adriatic and the European plates and associated horizontal stresses. This stylolitization provided an additional driving force for porosity loss by chemical compaction.

At all the deep wells (Lindau, Berlingen, Herdern and Kreuzlingen; z_{max}: 3080–3523 m) the pore-space is largely cemented by saddle dolomite (Fig. 3E–H and 4; Section 6.4). This pore-clogging mechanism

Table 5
Average matrix permeability in the Dolomit der Anhydritgruppe for the investigated wells across the Swiss Molasse Basin calculated from the various porosity logs and based on the correlation between porosity and permeability. The errors correspond to one standard deviation.

Well	Present-day depth[a] (m)	Maximum burial[b] (m)	Log k_{MSCL} (mD)	Log k_{NPHI} (mD)	Log k_{RHOB} (mD)	Log k_{DT} (mD)
Benken	880	~1930	–	−0.54 ± 1.06	−0.38 ± 0.77	−1.69 ± 0.62
Berlingen	2251	–	–	–	–	–
Böttstein	201	~1330	−0.50 ± 1.13	−0.34 ± 1.84	−0.58 ± 1.66	−0.63 ± 1.71
Bözberg	143	~1230	−0.14 ± 0.81	–	–	–
Entlebuch	5066	–	–	−2.75 ± 0.58	−2.69 ± 0.67	–
Herdern	2057	~3120	–	−1.95 ± 1.23	−0.96 ± 0.86	−2.56 ± 0.58
Kreuzlingen	2486	~3560	–	–	–	−2.57 ± 0.27
Leuggern	94	~1250	–	0.19 ± 1.11	0.41 ± 0.54	–
Lindau	2291	~3380	–	–	–	−2.92 ± 0.35
Pfaffnau	1616	–	–	–	–	−0.95 ± 0.82
Riniken	694	~1850	–	−1.48 ± 1.39	−1.15 ± 0.87	−1.18 ± 1.09
Schafisheim	1296	~2400	−3.02 ± 1.00	−2.75 ± 0.81	−2.98 ± 0.72	−2.48 ± 0.88
Schlattingen	1174	~2220	−0.67 ± 1.09	–	–	−2.10 ± 0.52
Siblingen	242	~1290	0.18 ± 0.96	0.34 ± 0.57	0.09 ± 0.53	−0.66 ± 0.66
Treycovagnes	2593	–	–	−2.64 ± 0.23	−1.64 ± 0.20	−3.29 ± 0.17
Weiach	893	~1980	−1.85 ± 1.52	−1.88 ± 1.17	−1.38 ± 1.19	−2.10 ± 1.10

[a] Average depth.
[b] Average depth at Miocene maximum burial according to studies by Nagra (2002) and Mazurek et al. (2006).

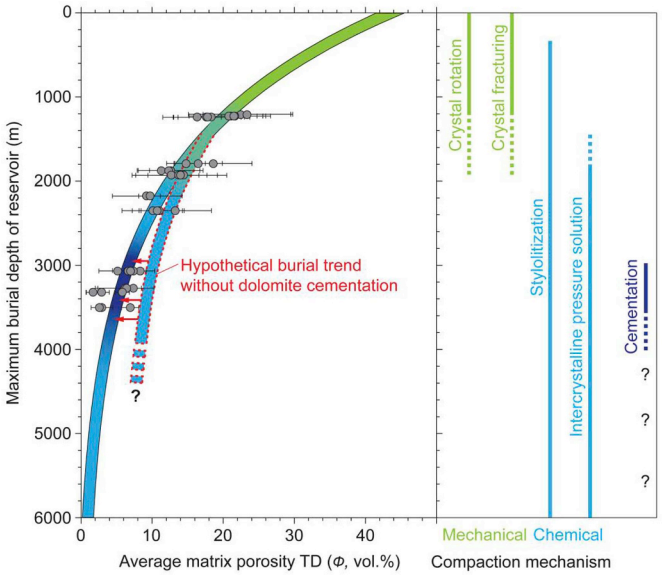

Fig. 13. Summary of mechanisms contributing to porosity loss in the Muschalkalk dolostones as a function of depth of burial in the Swiss Molasse Basin. The original uncemented mudstone fabrics are compacted by combined mechanical and chemical mechanisms at depths shallower than ~1200–1900 m and by purely chemical compaction at depths > 1900 m. Under very deep burial (i.e. ~3000–3500 m), pore-clogging by hydrothermal dolomite lowers porosities by more than would be expected if the rocks were affected solely by burial compaction (dashed red lines). (For interpretation of the references to colour in this figure legend, the reader is referred to the Web version of this article.)

overprints the pressure-solution-with-depth trend and leads to lower porosities than would be expected if the rocks were affected only by burial compaction (Fig. 13).

6.3. Comparison with South Florida dolostones

It is instructive to compare the porosity–depth trend of the Trigonodus Dolomit with the data of Schmoker and Halley (1982) for carbonates in South Florida (dotted curve in Fig. 11A). The South Florida dolostones represent a wide range of depositional facies and rock fabrics (shallow-shelf, subtidal, intertidal and supratidal environments) and, as was the case for the Trigonodus Dolomit, they were dolomitized during early diagenesis. However, dolomitization in South Florida resulted in overdolomitization and significant porosity loss. Accordingly, at depths shallower than 1700 m these dolostones show distinctly lower porosities than their undolomitized calcareous equivalents (Schmoker and Halley, 1982). The Trigonodus Dolomit lacks significant overdolomitization (Adams et al., 2018) and thus at shallow depths it has higher initial porosities than the South Florida dolostones. Schmoker and Halley (1982) also suggest an exponential decrease of dolostone porosity with increasing overburden, however, compactional porosity loss is distinctly slower and steadier than in the Trigonodus Dolomit. Consequently, the two curves intersect at around 900 m depth, and thereafter the Trigonodus Dolomit shows lower porosities (Fig. 11A). We attribute these differences in compaction behaviour to differences in four key parameters: (1) the depositional facies and associated rock fabrics, (2) the early diagenetic history of the rocks, (3) the tectonic setting and (4) pore-clogging by saddle dolomite, as discussed in the following.

First, Scholle and Halley (1985) have shown that coarse-grained fabrics (e.g. reefs, carbonate sand bodies, oolites) tend to retain porosity in the subsurface, whereas finer-grained fabrics such as the lagoonal muds of the Trigonodus Dolomit (Adams and Diamond, 2018), preferentially lose porosity during burial diagenesis.

Second, according to Purser (1978), early diagenetic lithification tends to retard or preclude subsequent mechanical and chemical compaction. Although overdolomitization reduced porosity in the South Florida dolostones, it formed a stable, supporting framework in the rock that retarded compactional porosity loss. In contrast, the lack of cementation during dolomitization of the Trigonodus Dolomit rendered its fabrics more susceptible to burial compaction.

Third, the South Florida basin is situated in a passive-margin setting where influences of tectonism are minimal. In contrast, the Swiss Molasse Basin is situated in the foreland of the European–Adriatic plate collision zone and thus it has been subjected to subhorizontal far-field compressive stresses along the NNW–SSE axis of plate convergence. The tectonic stylolites in the Upper Muschelkalk dolostones are interpreted to have formed as a result of this still on-going subhorizontal compression. The abundance of tectonic stylolites in all the investigated wells (Fig. 6) shows that they are an important additional mechanism for porosity loss via pressure solution and potentially cementation.

Fourth, as stated in Section 6.2, under deep burial (z_{max} ~3080–3523 m) the intercrystalline and separate-vug pores in the Trigonodus Dolomit are largely filled by saddle dolomite. This additional reduction in porosity is presumably another difference with respect to the South Florida samples, as Schmoker and Halley (1982) did

not specifically mention the presence of cements.

6.4. Significance of saddle dolomite cements

Generally, saddle dolomites can form by two different processes: First, in dolostones undergoing intense chemical compaction, they represent the reprecipitated product of pressure solution (Machel, 1987; Machel and Anderson, 1989). However, saddle dolomite can also form from influx of externally-derived hydrothermal fluids, as reported by Davies and Smith (2006) and Petts et al. (2017). The saddle dolomites in the Trigonodus Dolomit formed at temperatures of 142–161 °C (based on fluid inclusion analyses; Aschwanden, 2017), i.e. at ~20–40 °C higher than the estimated maximum formation temperature reached during the burial and exhumation history (Fig. 3D; Nagra, 2002). The influxing fluids were basement waters with $\delta^{18}O$ of −2.0–9.0‰ VSMOW and high $^{87}Sr/^{86}Sr$ ratios of ~0.7131 (Aschwanden, 2017). Thus, they are hydrothermal dolomites in the sense of Davies and Smith (2006). The basement water likely ascended along cross-formation faults that hydraulically connect the crystalline basement and the overlying Muschelkalk, resulting in dolomite precipitation upon mixing of the waters. This implies that the associated pore-clogging is restricted to the vicinity of such deep-seated tectonic structures. Although knowledge of the spatial distribution and extent of these structures in the deep basin is scant, the occurrence of saddle dolomite at all the deep wells in the NE Swiss Molasse Basin (Lindau, Berlingen, Kreuzlingen, Herdern; Fig. 1) suggests that pore-clogging by saddle dolomite may be regionally widespread.

6.5. Lack of pressure-solution cements

Conventionally, pressure solution implies that the material dissolved at pressure solution surfaces moves away from the site of dissolution and reprecipitates as pore-clogging cement in the immediate vicinity, where the stress is lower. However, there are only very few studies in which these expected links between pressure solution, cementation, and porosity loss can be demonstrated (Scholle and Halley, 1985).

In the Trigonodus Dolomit there is clear petrographic evidence for intense chemical compaction by pressure solution under deep burial conditions, yet these rocks lack the corresponding cements. This phenomenon was also observed in the Alpena limestone, Michigan Basin, by Buxton and Sibley (1981). There the rocks are pervasively affected by pressure solution (i.e. they show fitted fabric textures), but the dissolved material is not locally reprecipitated. Buxton and Sibley (1981) inferred from the lack of cement that advection of pore fluid must have been the dominant solute-transport mechanism in the Alpena limestone. It follows that the rate of fluid advection must have been greater than the rate of solute diffusion away from sites of dissolution and consequently solute concentrations could not reach supersaturation in the pore fluids. However, a problem arises when dealing with weakly permeable rocks, such as the Trigonodus Dolomit at great depth. In these rocks advective transport through the rock matrix is rather slow and the continuous addition of solutes from pressure solution is likely to cause dolomite supersaturation in the migrating fluids after only short transport distances. The problem could conceivably be overcome in a regional recharge–discharge hydrogeological system with high hydrostatic gradients, which drive rapid advective flow of significant masses of groundwater through the rock matrix of the dolostones during the periods of intense pressure solution (i.e. under deep burial conditions). However, from hydrodynamic and petrophysical perspectives it seems unlikely that such conditions could have prevailed in the deeply buried Trigonodus Dolomit. Alternatively, the absence of pressure-solution cement may be due to kinetic factors (e.g. the presence of sulphate), which inhibited dolomite precipitation at low levels of supersaturation. However, it is notable that the precipitation of saddle dolomite, which was introduced by an externally-derived fluid and which deposited at high supersaturation due to fluid mixing (Section 6.4), was not kinetically inhibited. The lack of pressure-solution cements in these dolostones therefore remains an unresolved problem.

7. Conclusions

The best-fit regressions describing the porosity–depth and permeability–depth trends of the Upper Muschelkalk dolostones in the Swiss Molasse Basin are exponential curves. These trends are due to the cumulative effects of sedimentary inheritance and early diagenesis overprinted by a series of compaction and cementation processes, each operating over certain depth ranges: (1) The sedimentary inheritance provided fine-grained, largely uncemented mudstone fabrics that are particularly susceptible to compactional porosity loss; (2) Early diagenetic dolomitization provided a porous and permeable matrix (40–45 vol%. and ~100 mD) without significant overdolomitization and hence without the associated strengthening of the rock fabric; (3) During progressive burial to ~1200–1900 m depth, grain rearrangement and breakage, as well as closure of large intercrystalline pores by combined mechanical collapse and pressure solution reduced the matrix porosity and permeability to 13–20 vol% and 0.2–2 mD, respectively; (4) At depths greater than ~1900 m, individual dolomite crystals became interlocked, precluding further mechanical collapse. Compaction therefore continued solely via pressure solution along dolomite crystal-to-crystal contacts and along stylolites. The extent of pressure solution was controlled in part by the burial depth and its associated vertical stresses (which created diagenetic stylolites), but also in part by the horizontal, compressive stresses (which created tectonic stylolites) due to the tectonic setting of the basin in the foreland of a plate collision zone. Under deep burial (i.e. ~3000–3500 m), the closeness of crystal packing increased via pervasive interparticle pressure solution, producing tightly interlocked, "fitted" fabrics containing few intercrystalline pores; (5) Within this deepest burial range (~3000–3500 m) much of the residual pore-space was clogged by saddle dolomite, which precipitated upon influx of hydrothermal water ascending along faults from the crystalline basement. This overprinting of the pressure-solution-with-depth trend by cement eliminated all pores larger than 100 μm^2, resulting in matrix porosity and permeability values of 2–8 vol% and 0.0007–0.01 mD, respectively.

Acknowledgements

We thank the Swiss National Cooperative for the Disposal of Radioactive Waste (Nagra) and the Corporation for Swiss Petroleum (SEAG) for generously providing access to their drill cores and borehole logs. We appreciate the helpful comments by two anonymous journal reviewers. This research was conducted within the framework of the Swiss Competence Center for Energy Research – Supply of Energy (SCCER-SoE), with support of the Swiss National Science Foundation via NRP70 ″Energy Turnaround" Grant 407040_153889 to L.W.D.

Appendix A. Supplementary data

Supplementary data to this article can be found online at https://doi.org/10.1016/j.marpetgeo.2018.10.055.

Appendix

Table A.1
Compilation of wells (ranked according to penetration depth) and wireline logs investigated in this study.

Well	Current depth TD (m)	Current depth DAG (m)	Maximum burial depth TD (m)[5]	Maximum burial depth DAG (m)[5]	Basis for estimating lithological boundaries	Drill core examined in this study	Wireline logs[4]
Leuggern (LEU)	48.5–58.2	87.9–100.4	1139–1148	1178–1191	WL; Nagra (1991)	–	LDT, CNT
Bözberg (BOZ)	58.4–96.0	136.0–148.8	1149–1186	1226–1239	DC	38 m TD; 13 m DAG	–
Böttstein (BOE)	121.9–150.8	197.2–204.6	1212–1241	1287–1295	WL; Nagra (1985)	29 m TD; 7 m DAG	LDT, CNT, DT
Siblingen (SIB)	177.0–207.8	233.7–249.4	1267–1298	1324–1340	WL; Nagra (1992b)	–	LDT, CNT, DT
Riniken (RIN)	616.0–652.4	688.5–698.5	1775–1811	1848–1858	WL; Nagra (1990)	–	LDT, CNT, DT
Benken (BEN)	811.4–848.5	874.3–886.3	1856–1894	1919–1931	WL; Nagra (2001)	37 m TD; 12 m DAG	LDT, CNT, DT
Weiach (WEI)	819.1–857.1	887.9–897.7	1909–1947	1978–1988	WL; Nagra (1989)	38 m TD; 10 m DAG	LDT, CNT, DT
Schlattingen (SLA)	1112.0–1145.3	1169.5–1179.1	2202–2235	2260–2269	DC	24 m TD; 10 m DAG	DT
Schafisheim (SHA)	1228.3–1256.3	1287.7–1305.0	2338–2366	2398–2415	DC & WL; Nagra (1992a)	10 m TD; 18 m DAG	LDT, CNT, DT
Pfaffnau (PFA)	~1546–1575	~1610–1622[1]	~2636–2665	~2700–2712	WL; Büchi et al. (1965)	13 m TD	DT
Herdern (HER)	1990–2020	~2052–2062	~3053–3083	~3115–3125	WL	11 m TD	LDT, CNT, DT
Berlingen (BER)	~2179–2191	~2245–2257[1]	~3266–3278	~3332–3344	Büchi et al. (1965)	11 m TD	DT
Kreuzlingen (KRE)	~2415–2433[2]	~2480–2492[1]	~3505–3523	~3558–3570	DC; Büchi et al. (1965)	13 m TD	DT
Lindau (LIN)	~2225–2267[2]	~2285–2297[1]	~3315–3357	~3375–3387	DC; Büchi et al. (1965)	42 m TD	DT
Treycovagnes (TRE)	~2530–2546	~2584–2601	[6]	[6]	WL; Sommaruga (1997)	–	LDT, CNT, DT
Entlebuch (ENT)	~5050–5082[3]		[6]		Vollmayr & Wendt (1987)	–	LDT, CNT

TD: Trigonodus Dolomit; DAG: Dolomit der Anhydritgruppe.
WL: wireline logs; DC: drill core; LDT: density logs; CNT: neutron porosity logs; DT: sonic logs.
[1] Exact depth of base of DAG cannot be determined precisely. Tabulated values are rough estimates.
[2] Exact depth of base of TD cannot be determined precisely. Tabulated values are minima based on our drill core investigations.
[3] Depth range corresponds to entire Muschelkalk. Further subdivision is not possible.
[4] Additional logs not mentioned in the Table but available for each well include caliper and natural-gamma logs.
[5] Values represent best estimates based on published age–burial curves from Nagra (2002).
[6] No indication on maximum burial depth.

Table A.2
Percentage of geophysical borehole logs used for porosity determination after discarding values affected by borehole roughness or breakouts.

Well	Trigonodus Dolomit			Dolomit der Anhydritgruppe		
	LDL	CNL	DT	LDL	CNL	DT
Leuggern	80	86	–	85	87	–
Böttstein	100	100	99	84	84	84
Siblingen	98	98	100	100	100	100
Riniken	81	81	81	100	100	100
Benken	100	100	100	100	100	100
Weiach	93	93	93	100	100	100
Schlattingen	–	–	100	–	–	100
Schafisheim	92	92	92	100	100	100
Pfaffnau	–	–	100	–	–	30
Herdern	59	71	97	13	54	63
Berlingen	–	–	82	–	–	–
Kreuzlingen	–	–	100	–	–	100
Lindau	–	–	100	–	–	100
Treycovagnes	91	86	89	100	100	100
Entlebuch	76	85	–	76	85	–

LDL: density log; CNL: neutron porosity log; DT: sonic log.

References

Adams, A., Diamond, L.W., 2018. Early diagenesis driven by widespread meteoric infiltration of a Central European carbonate ramp: a reinterpretation of the Upper Muschelkalk. Sediment. Geol. 362, 37–52.

Adams, A., Diamond, L.W., Aschwanden, L., 2018. Dolomitization by hypersaline reflux into dense groundwaters as revealed by vertical trends in Sr- and O-isotopes: upper Muschelkalk, Switzerland. Sedimentology. https://doi.org/10.1111/sed.12530. (in press).

Aschwanden, L., 2017. Evolution of Matrix Porosity and Permeability in Dolostones of the Middle- and Upper Muschelkalk. Swiss Molasse Basin: Doctoral dissertation. University of Bern, Bern 157 pp.

Bakker, R.J., Diamond, L.W., 2006. Estimation of volume fractions of liquid and vapor phases in fluid inclusions, and definition of inclusion shapes. Am. Mineral. 91, 635–657.

Bathurst, R.G.C., 1971. Carbonate Sediments and Their Diagenesis, Developments in Sedimentology. Elsevier, Amsterdam-Oxford-New York.

Berman, R.G., 1988. Internally-consistent thermodynamic data for minerals in the system Na_2O-K_2O-CaO-M_gO-FeO-Fe_2O_3-Al_2O_3-SiO_2-TiO_2-H_2O-CO_2. J. Petrol. 29 (2), 445–522.

Büchi, U.P., Lemcke, K., Wiener, G., Zimdars, J., 1965. Geologische Ergebnisse der Erdölexploration auf das Mesozoikum im Untergrund des schweizerischen Molassebeckens. Bulletin der Vereinigung Schweizerischer Petroleum-Geologen und -Ingenieure 32 (82), 7–38.

Buxton, T.M., Sibley, D.F., 1981. Pressure solution features in a shallow buried limestone. J. Sediment. Res. 51 (1), 19–26.

Chadwick, A., Arts, R., Bernstone, C., May, F., Thibeau, S., Zweigel, P., 2007. Best Practice for the Storage of CO_2 in Saline Aquifers - Observations and Guidelines from the SACS and CO2STORE Projects. British Geological Survey, Nottingham.

Chevalier, G., Diamond, L.W., Leu, W., 2010. Potential for deep geological sequestration of CO_2 in Switzerland: a first appraisal. Swiss J. Geosci. 103 (3), 427–455.

Choquette, P.W., Steinen, R.P., 1980. Mississippian non-supratidal dolomite, Ste. Genevieve Limestone, Illinois Basin: evidence for mixed-water dolomitization. In: In: Zenger, D.H., Dunham, J.B., Ethington, R.L. (Eds.), Concepts and Models of Dolomitization, vol. 28. SEPM Special Publication, pp. 163–196.

Croizé, D., Renard, F., Gratier, J.P., 2013. Compaction and porosity reduction in carbonates: a review of observations, theory, and experiments. Adv. Geophys. 54, 181–238.

Davies, G.R., Smith Jr., L.B., 2006. Structurally controlled hydrothermal dolomite reservoir facies: an overview. AAPG Bull. 90 (11), 1641–1690.

Ehrenberg, S.N., Nadeau, P.H., 2005. Sandstone vs. carbonate petroleum reservoirs: a global perspective on porosity-depth and porosity-permeability relationships. AAPG (Am. Assoc. Pet. Geol.) Bull. 89 (4), 435–445.

Ehrenberg, S.N., Eberli, G.P., Keramati, M., Moallemi, S.A., 2006. Porosity–permeability relationships in interlayered limestone-dolostone reservoirs. AAPG (Am. Assoc. Pet. Geol.) Bull. 90 (1), 91–114.

Ehrenberg, S.N., 2006. Porosity destruction in carbonate platforms. J. Petrol. Geol. 29 (1), 41–52.

Goldscheider, N., Mádl-Szőnyi, J., Erőss, A., Schill, E., 2010. Review: thermal water resources in carbonate rock aquifers. Hydrogeol. J. 18 (6), 1303–1318.

Gregg, J.M., Sibley, D.F., 1984. Epigenetic dolomitization and the origin of xenotopic dolomite texture. J. Sediment. Petrol. 54, 908–931.

Hugman, R.H.H., Friedman, M., 1979. Effects of texture and composition on mechanical behavior of experimentally deformed carbonate rocks. AAPG (Am. Assoc. Pet. Geol.) Bull. 63 (9), 1478–1489.

Jordan, P., 2016. Reorganisation of the Triassic stratigraphic nomenclature of northern Switzerland: overview and the new Dinkelberg, Kaiseraugst and Zeglingen formations. Swiss J. Geosci. 109 (2), 241–255.

Kempf, O., Pfiffner, O.A., 2004. Early Tertiary evolution of the north alpine Foreland Basin of the Swiss Alps and adjoining areas. Basin Res. 16 (4), 549–567.

Laubscher, H., 1961. Die Fernschubhypothese der Jurafaltung. Eclogae Geol. Helv. 54, 221–281.

Logan, B.W., Semeniuk, V., 1976. Dynamic Metamorphism; Processes and Products in Devonian Carbonate Rocks, Canning Basin. Geological Society of Australia Special Publication, no. 16, Western Australia, pp. 138.

Loup, B., 1992. Mesozoic subsidence and stretching models of the lithosphere in Switzerland (Jura, Swiss Plateau and Helvetic realm). Eclogae Geol. Helv. 85, 541–572.

Machel, H.G., Anderson, J.H., 1989. Pervasive subsurface dolomitization of the Nisku formation in central Alberta. J. Sediment. Petrol. 59 (6), 891–911.

Machel, H.G., 1987. Saddle dolomite as a by-product of chemical compaction and thermochemical sulfate reduction. Geology 15, 936–940.

Machel, H.G., 2004. Concepts and Models of Dolomitisation: a Critical Reappraisal, vol. 235. Geological Society, London, Special Publications, pp. 7–63.

Mazurek, M., Hurford, A.J., Leu, W., 2006. Unravelling the multi-stage burial history of the Swiss Molasse Basin: integration of apatite fission track, vitrinite reflectance and biomarker isomerisation analysis. Basin Res. 18, 27–50.

Moore, C.H., 2001. Carbonate Reservoirs: Porosity Evolution and Diagenesis in a Sequence Stratigraphic Framework, Developments in Sedimentology, vol. 55 Elsevier, Amsterdam-Oxford-New York.

Morgan, D.J., Jerram, D.A., 2006. On estimating crystal shape for crystal size distribution analysis. J. Volcanol. Geoth. Res. 154, 1–7.

Nagra, 1985. Sondierbohrung Böttstein Untersuchungsbericht - Nagra Technischer Bericht NTB 85-01. Nagra, Baden 190 pp.

Nagra, 1989. Sondierbohrung Weiach Untersuchungsbericht Beilagenband - Nagra Technischer Bericht NTB 88-08. Nagra, Baden 183 pp.

Nagra, 1990. Sondierbohrung Riniken Untersuchungsbericht Beilagenband - Nagra Technischer Bericht NTB 88-09. Nagra, Baden 125 pp.

Nagra, 1991. Sondierbohrung Leuggern Untersuchungsbericht - Nagra Technischer Bericht NTB 88-10. Nagra, Wettingen 168 pp.

Nagra, 1992a. Sondierbohrung Schafisheim Untersuchungsbericht Beilagenband - Nagra Technischer Bericht NTB 88-11. Nagra, Wettingen 183 pp.

Nagra, 1992b. Sondierbohrung Siblingen Untersuchungsbericht - Nagra Technischer Bericht NTB 90-34. Nagra, Wettingen 130 pp.

Nagra, 2001. Sondierbohrung Benken Untersuchungsbericht Beilagenband - Nagra Technischer Bericht NTB 00-01. Nagra, Wettingen 288 pp.

Nagra, 2002. Projekt Opalinuston, Synthese der geowissenschaftlichen Untersuchungsergebnisse – Nagra Technischer Bericht NTB 02-03, Wettingen, Nagra. 659 pp.

Palchik, V., Hatzor, Y.H., 2002. Crack damage stress as a composite function of porosity and elastic matrix stiffness in dolomites and limestones. Eng. Geol. 63, 233–245.

Petts, D.C., Saso, J.K., Diamond, L.W., Aschwanden, L., Al, T.A., Jensen, M., 2017. The Source and Evolution of Paleofluids Responsible for Secondary Minerals in Low-permeability Ordovician Limestones of the Michigan Basin. Applied Geochemistry (in press).

Pfiffner, O.A., Erard, P.F., Stäuble, M., 1997. Two cross sections through the Swiss Molasse basin (lines E4-E6, W1, W7-W10). In: Pfiffner, O.A., Lehner, P., Heitzmann, P., Müller, S., Steck, A. (Eds.), Results of NRP 20 - Deep Structure of the Swiss Alps: Basel, Birkhäuser, pp. 64–72.

Pfiffner, O.A., 2014. Geology of the Alps. John Wiley & Sons 368 pp.

Purser, B.H., Brown, A., Aissaoui, D.M., 1994. Nature, origins and porosity in dolomites. In: In: Purser, B., Tucker, M., Zenger, D. (Eds.), Dolomites: International Association of Sedimentologists Special Publication, vol. 21. pp. 283–308.

Purser, B.H., 1978. Early diagenesis and the preservation of porosity in Jurassic limestones. J. Petrol. Geol. 1 (2), 83–94.

Saller, A.H., Henderson, N., 1998. Distribution of porosity and permeability in platform dolomites: insight from the Permian of west Texas. AAPG (Am. Assoc. Pet. Geol.) Bull. 82 (8), 1528–1550.

Schauer, M., Aigner, T., 1997. Cycle stacking pattern, diagenesis and reservoir geology of peritidal dolostones, Trigonodus-Dolomite, Upper Muschelkalk (Middle Triassic, SW-Germany). Facies 37, 99–114.

Schlumberger, 1989. Log Interpretation Principles/Applications. Schlumberger Educational Services, Houston.

Schmoker, J.W., Halley, R.B., 1982. Carbonate porosity versus depth: a predictable relation for south Florida. AAPG (Am. Assoc. Pet. Geol.) Bull. 66 (12), 2561–2570.

Scholle, P.A., Halley, R.B., 1985. Burial diagenesis: Out of sight, out of mind!. In: In: Schneidermann, N., Harris, P.M. (Eds.), Carbonate Cements, vol. 36. SEPM Special Publication, pp. 309–334.

Sibley, D.F., Gregg, J.M., 1987. Classification of dolomite rock textures. J. Sediment. Petrol. 57, 967–975.

Sommaruga, A., Eichenberger, U., Marillier, F., 2012. Seismic Atlas of the Swiss Molasse Basin. Federal Office of Topography swisstopo, Wabern.

Sommaruga, A., 1997. Geology of the Central Jura and the Molasse Basin: New Insight into an Evaporite-based Foreland Fold and Thrust Belt. Doctoral dissertation. University of Neuchâtel, Neuchâtel 1365 pp.

Sun, S.Q., 1995. Dolomite reservoirs: porosity evolution and reservoir characteristics. AAPG (Am. Assoc. Pet. Geol.) Bull. 79 (2), 186–204.

Tada, R., Siever, R., 1989. Pressure solution during diagenesis. Annu. Rev. Earth Planet Sci. 17, 89–118.

Vollmayr, T., Wendt, A., 1987. Die Erdgasbohrung Entlebuch 1, ein Tiefenaufschluss am Alpennordrand. Bulletin der Vereinigung Schweizerischen Petroleum-Geologen und-Ingenieure 53 (125), 67–79.

Warren, J.E., Price, H.S., 1961. Flow in heterogeneous porous media. Soc. Petrol. Eng. J. 1 (3), 153–169.

Wildi, W., Funk, H.P., Loup, B., Amato, E., Huggenberger, P., 1989. Mesozoic subsidence history of the European marginal shelves of the alpine Tethys (Helvetic realm, Swiss plateau and Jura). Eclogae Geol. Helv. 82, 817–840.

Ziegler, P.A., 1990. Geological Atlas of Western and Central Europe, 2nd Ed. Shell Internationale Petroleum Maatschappij B.V.: Bath. Geological Society Publishing House 239 pp.